ORNL/TM-2012/430

High-Temperature Fluoride Salt Test Loop

Graydon L. Yoder, Jr.
Adam Aaron
Burns Cunningham
David Fugate
David Holcomb
Roger Kisner
Fred Peretz
Kevin Robb
Dane Wilson

DECEMBER 2015

OAK RIDGE NATIONAL LABORATORY
MANAGED BY UT-BATTELLE FOR THE US DEPARTMENT OF ENERGY

ORNL/TM-2012/430

Reactor and Nuclear Systems Division

HIGH-TEMPERATURE FLUORIDE SALT TEST LOOP

Graydon L. Yoder, Jr.
Adam Aaron
Burns Cunningham
David Fugate
David Holcomb
Roger Kisner
Fred Peretz
Kevin Robb
Dane Wilson

Date Published: December 2015

Prepared by
OAK RIDGE NATIONAL LABORATORY
Oak Ridge, TN 37831-6283
managed by
UT-BATTELLE, LLC
for the
US DEPARTMENT OF ENERGY
under contract DE-AC05-00OR22725

CONTENTS

LIST OF FIGURES

LIST OF TABLES

ACRONYMS AND ABBREVIATIONS

CF	conflat
FHR	fluoride salt high-temperature reactor
HX	heat exchanger
ID	inside diameter
NPT	National Pipe Thread
OD	outside diameter
PB-AHTR	pebble bed–advanced high-temperature reactor
PLC	programmable logic control
UC–Berkeley	University of California–Berkeley

EXECUTIVE SUMMARY

The need for high-temperature (greater than 600°C [greater than 1100°F]) energy exchange and delivery systems is significantly increasing as both the United States and the rest of the world strive to improve energy efficiency and develop alternatives to petroleum-based fuels. Liquid fluoride salts are one of the few energy transport fluids that have the capability of operating at high temperatures in combination with low system pressures. The fluoride salt-cooled high-temperature reactor (FHR) design uses fluoride salt to remove core heat and interface with a power conversion system. Although a significant amount of experimentation has been performed with these salts, specific aspects of this reactor concept will require experimental confirmation during the development process.

The experimental facility described in this report has been constructed to support the development of the FHR reactor concept. The facility is capable of operating at up to 700°C (greater than 1290°F) and incorporates a centrifugal pump to circulate FLiNaK salt through a removable test section. A unique inductive heating technique is used to apply heat to the test section, allowing heat transfer testing to be performed. An air-cooled heat exchanger removes heat that was added to the test section. Supporting loop infrastructure includes a pressure control system; trace heating system; and complement of instrumentation to measure salt flow, temperatures, and pressures around the loop.

The initial planned experiment is aimed at measuring fluoride salt heat transfer inside a heated pebble bed similar to that used for the core of the pebble bed–advanced high-temperature reactor.

This document describes the details of the loop design, auxiliary systems used to support the facility, inductive heating system, and initial planned experiment.

1. INTRODUCTION

Effective high-temperature thermal energy exchange and delivery at temperatures over 600ºC (1100°F) has the potential for significant impact by improving system efficiencies and reducing system size, resulting in reduced capital and operating costs of energy conversion and transport systems. It is one of the key technologies necessary for efficient hydrogen production and could potentially enhance efficiencies of high-temperature solar systems. Today there are no standard, commercially available high-performance heat transfer fluids above 600ºC. High pressures associated with water and gaseous coolants (such as helium) at elevated temperatures impose limiting design conditions for the materials in most energy systems. Liquid salts offer high-temperature capabilities at low vapor pressures, good heat transport properties, and reasonable costs and are therefore leading candidate fluids for next-generation energy production. Liquid-fluoride-salt-cooled, graphite-moderated reactors, referred to as fluoride salt high-temperature reactors (FHRs), are specifically designed to exploit the excellent heat transfer properties of liquid fluoride salts while maximizing their thermal efficiency and minimizing cost. The FHR's outstanding heat transfer properties, combined with its fully passive safety, make this reactor the most technologically desirable nuclear power reactor class for next-generation energy production.

Multiple FHR designs are presently being considered. These range from the pebble bed–advanced high-temperature reactor (PB-AHTR) design originally developed by the University of California–Berkeley (UC-Berkeley)[1] to the small advanced high-temperature reactor [2] and the large-scale advanced high-temperature reactor both being developed at Oak Ridge National Laboratory.[3] The value of high-temperature, molten-salt-cooled reactors is also recognized internationally, and the Czech Republic, France, India, and China all have salt-cooled reactor development under way, with China planning on completing an FHR test reactor in the 2015–2017 timeframe.

The initial experiment planned for the liquid salt test loop is to demonstrate the heat transfer performance of liquid fluoride salt in a fixed pebble bed. The test pebble bed resembles that planned for the PB-AHTR. The 2008 core design of the PB-AHTR features multiple 20 cm (7.9 in.) diameter, 3.2 m (126 in.) long fuel channels with 3 cm (1.2 in.) diameter graphite-based fuel pebbles slowly circulating up through the core. Molten salt coolant (FLiBe) at 700ºC (1290°F) flows concurrently (at significantly higher velocity) with the pebbles and is used to remove heat generated in the reactor core (approximately 1285 W/pebble [4385 Btu/h/pebble]) and supply it to a power conversion system. The experiment being developed focuses on thermal and hydraulic behavior of a static pebble bed using a convective salt loop to provide prototypic fluid conditions to the bed and a unique inductive heating technique to provide prototypic heating in the pebbles. The PB-AHTR design is discussed in detail in ref. [1] and shown schematically in Fig. 1.

The facility design is sufficiently versatile to allow a variety of other experimentation to be performed in the future, serving as the centerpiece of an FHR component test facility. The facility can accommodate testing of scaled reactor components or subcomponents such as flow diodes, salt-to-salt heat exchangers, and improved pump designs as well as testing of refueling equipment, high-temperature instrumentation, and other reactor core designs.

2. PEBBLE BED HEAT TRANSFER

The initial test program is designed to evaluate the heat transfer in a static pebble bed. An extensive amount of work has been done examining the performance of packed and fluidized beds in support of the chemical and petroleum industries, and entire texts are devoted to this subject.[4,5] Packed beds are used to enhance both mass and heat transfer performance, and specific packing designs have been developed over the years to optimize these characteristics. In most packed bed systems used to improve heat transfer performance, heat is added externally, and the packing is used to augment heat transfer in the channel.

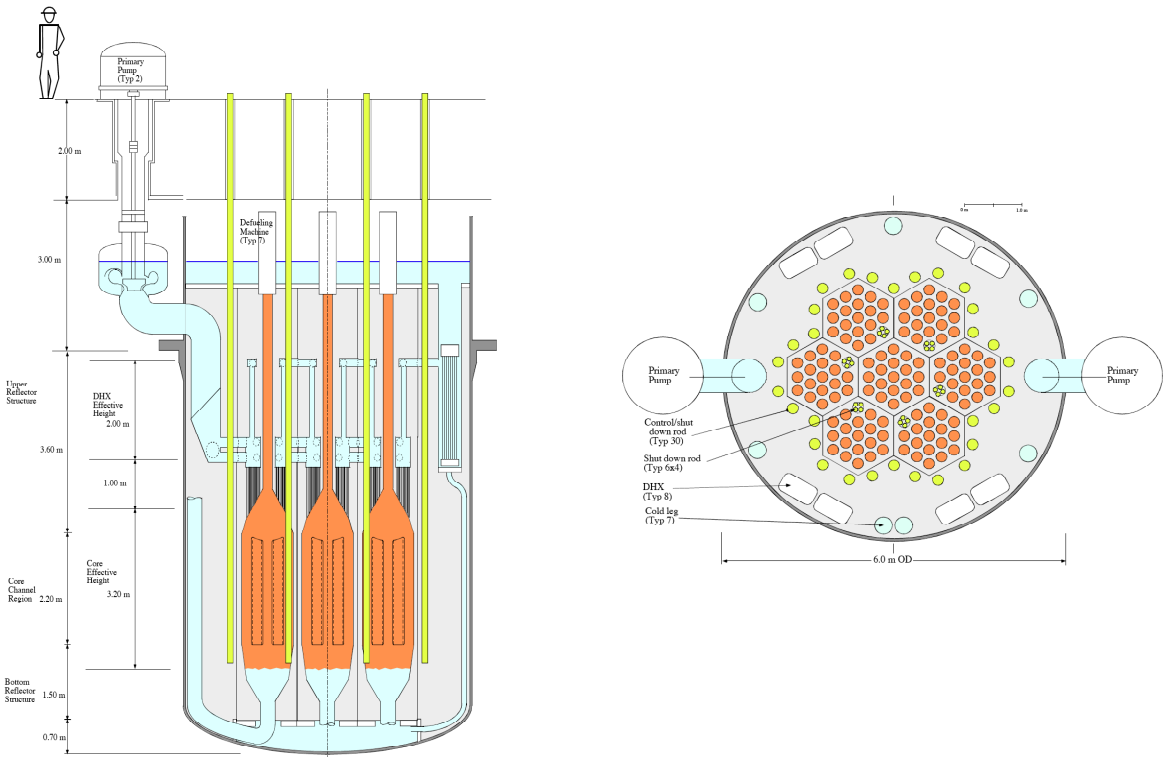

Fig. 1. PB-AHTR concept (drawing taken from ref. 1).

The existing body of literature includes studies investigating radiative as well as convective transport within the bed, [6,7] the influence of the wall on geometrical packing, [8,9] and details of the turbulence within the bed, [10,11] as well as other phenomena. A unique feature of pebble-fueled reactor systems is that heat is generated within the pebbles themselves, and the heat transfer from the pebble to the molten salt dictates the fuel temperature, ultimately establishing reactor operating limits.

Pebble bed studies have also been performed to support nuclear reactor systems. The South African pebble bed modular gas-cooled reactor project has performed pebble bed experiments that use electrical resistance heaters imbedded in a square-lattice pebble bed to apply the appropriate amount of bulk heating to the circulating helium. [12] Experimental efforts at UC-Berkeley supporting the PB-AHTR have concentrated on using commercial heat transfer oils as a low-temperature simulant for molten salt and have allowed relevant fluid and heat transfer system design experiments to be performed at low temperatures. Experiments using more prototypic materials, temperature, and fluid heating are the next major demonstration step in proving the viability and capabilities of this reactor concept and are needed to guide the design and prepare functional test and reliability data for reactor licensing.

The inductive heating techniques that we are using in this project will directly heat a prototypic randomly packed pebble bed geometry and will appropriately simulate the internal heating in a pebble-fueled reactor. Although inductive heating is a very common industrial heating method and is used in the foundry industries for melting metals, a very limited amount of work has been performed examining the use of inductive heating in regular packed bed type systems.

3. EXPERIMENTAL DESIGN

3.1 LOOP CONSTRUCTION

Figure 2 shows a schematic of the loop. A vertical shaft electric-motor-driven centrifugal pump circulates salt through an inductively heated test section that contains the pebble bed. The pump is housed in a sump tank where argon overpressure is applied to force salt into the loop during operation. A surge tank at the top of the loop also contains an argon/salt interface and is used to establish loop operating pressure. An air-cooled heat exchanger removes heat added by the inductive heating system. Trace heaters are located on all piping and components to heat the loop above FLiNaK melt temperature (454°C) before salt is introduced into the loop. The trace heating also ensures that the salt never freezes in the loop. Before salt is transferred into the loop storage tank, moisture is removed from the salt by heating it in a separate processing crucible and holding it at a temperature below the melting point. The salt is then melted, and hydrogen fluoride gas is bubbled through the melt to remove moisture. (Detailed discussion of this process in not included in this document.) Once purified, the salt is transferred to the loop storage tank using differential gas pressure. The storage tank is designed to permit salt freezing and allows long-term salt storage. Once melted in the storage tank, the salt is transferred into the pump sump tank via gas pressure differentials. Once salt is in the loop, the sump tank is pressurized with argon, and the surge tank is vented, forcing the salt up into the loop until the desired liquid level is reached in the surge tank. Loop instrumentation includes salt flow rate, pump discharge pressure, tank gas pressures, salt temperatures in the pebble bed, and appropriate temperature measurements of loop piping and components to control trace heating. The inductive heating power level is measured as well as air temperature across the heat exchanger.

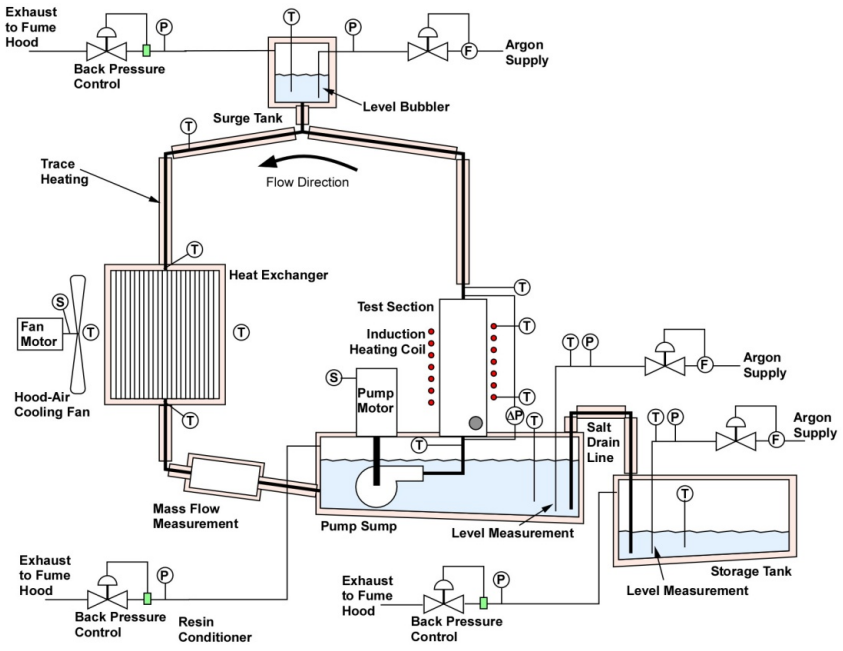

Fig. 2. Liquid Salt Test Loop schematic.

The loop and storage tank, except for the test section, are constructed of alloy 600 selected for compatibility with molten fluoride salts, availability of required forms, and cost. Hastelloy N or MONICR (a Czech Republic version of Hastelloy N) are the preferred alloys; however, the limited availability of these alloys made their cost prohibitive for use in this project. The salt-containing portion of the loop is of

all-welded construction where possible. Flanged connections, penetrations, and pump seals are at elevations above the salt level, providing only gas sealing whenever feasible. However, two flanges in the system are designed to contact the salt and effect a salt seal, one at the top of the test section designed to transition from the SiC test section and the alloy 600 piping and one in the piping near the surge tank to allow piping alignment with the test section. Although the salt proposed for the PB-AHTR is FLiBe, the salt used in this experiment is FLiNaK in order to eliminate any safety issues that might arise due to the presence of beryllium. The loop is designed to supply a known flow rate and temperature of FLiNaK to the test section and operates at near atmospheric pressure. Lines are sloped to ensure salt draining and allow a 100% salt fill of the loop. The loop uses an ultrapure argon cover gas to prevent moisture and oxygen from entering the system. A photo of the as-built loop is shown in Fig. 3. The storage tank is at the bottom center of the picture, the pump sump tank at the middle left, the heat exchanger and ductwork at the upper right, and the surge tank just to the left of the heat exchanger.

Fig. 3. Picture of loop in hood.

3.2 FLiNaK SALT

A comparison of thermophysical properties for FLiNaK, FLiBe, and other coolant fluids is presented in Table 1 for comparison. LiF, NaF, and KF salts were purchased from Wilson Scientific in quantities proportional to those needed to make FLiNaK eutectic salt (46.5 mol % LiF-11.5 mol % NaF-42 mol % KF). These salts were industrial grade and must be purified to minimize corrosion. The salts will be purified in 150 kg (330 lb) batches, enough for one complete fill of the loop. Discussion of the purification process is outside the scope of this document.

Table 1. Comparison of FLiBe thermophysical properties with that of other heat transfer media

Fluid	T_{melt}, °C (°F)	T_{boil}, °C (°F)	ρ, kg/m^3 (lbm/ft^3)	c_p, J/kg°C (Btu/lb°F)	μ, Pa-s (lbm/fth)	k, W/m°C (Btu/fth°F)
$^7Li_2BeF_4$ (FLiBe)	459 (858)	1,430 (2,606)	1,940 (121)	2,386 (0.57)	6.78×10^{-3} (16.4)	1.1 (0.636)
LiF-NaF-KF (FLiNaK)	454 (849)	1,570 (2,858)	2,019 (126)	1,884 (0.45)	2.91×10^{-3} (7.04)	0.8 (0.462)
Sodium (550°C)	97.8 (208)	883 (1,531)	817 (51)	1,263 (0.30)	2.53×10^{-4} (0.61)	65.0 (37.6)
Lead (600°C)	328 (622)	1,750 (3,182)	10,270 (641)	1,549 (0.37)	1.6×10^{-3} (3.87)	15.1 (8.72)
Helium (7.5 MPa)	—	—	3.8 (0.24)	5,189 (1.24)	4.53×10^{-5} (0.12)	0.36 (0.208)
Water (7.5 MPa)	0	291 (556)	732 (45.7)	5,484 (1.31)	8.9×10^{-5} (0.22)	0.56 (0.324)
Water (Atm.)	0	100 (212)	998 (62.3)	4,183 (1.00)	2.8×10^{-4} (0.68)	0.6 (0.347)
Graphite	—	—	1,700 (106)	—		200.0 (115.6)

3.3 SURGE TANK

A small surge tank located at the top of the loop is used to allow argon to be vented during loop fill and provide space for salt expansion and contraction during loop operation (Fig. 4). A slight argon overpressure is maintained within the tank. The tank is constructed of 200 mm (8 in.) diameter schedule 40 pipe approximately 280 mm (11 in.) long. A hemispherical end cap forms the bottom of the tank. The tank is constructed of alloy 600 except for the conflat (CF)-type closure flanges, which are made of 304 stainless steel. The flange seal is made using either a fully annealed nickel or copper ring. The surge tank is designed to operate at 700°C (1290°F) at pressures below 0.20 MPa (15 psig). The top flange has seven penetrations that are all designed to extend above the flange a sufficient distance to remain cool enough during operation to use Teflon seals. Each tube is terminated at the top with Swagelok compression fittings. Two penetrations are used for the heated thermocouple level indicators, one is used for gas inlet, one for gas outlet, and one 8 mm (1.5 in.) diameter schedule 10 pipe extends to near the bottom of the tank and acts as a wave guide for a radar-based level detector. Two penetrations are spares. The tank is connected to the remainder of the loop through a short section of 25 mm (1 in.) schedule 40 pipe. The surge tank is attached to the loop framework through a lug and threaded rod to a spring hanger (Anvil International – Type C) that allows the tank to move freely in all directions to accommodate thermal expansion.

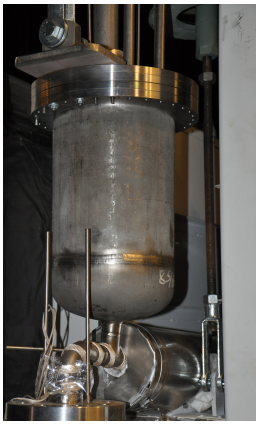

Fig. 4. Surge tank.

3.4 STORAGE TANK

The storage tank is designed to hold all of the 150 kg (330 lb) (75 L [2.65 ft^3]) of salt that will be used in the loop and allow it to freeze for long-term storage (Fig. 5) The tank has a volume of approximately 150 L (5.3 ft^3), so the salt occupies only 50% of the total volume. The tank is a horizontal cylinder with a diameter of 51 cm (20 in.) with a wall thickness of 6.4 mm (0.25 in.). A 30.5 mm (12 in.) CF-type flange and 203 mm (8 in.) schedule 40 pipe nozzle at the top of the tank allow access. The CF flange has eight tubing penetrations similar to those discussed above for the surge tank. Two penetrations are used for the heated thermocouple level indicators, one is used for gas inlet, one for gas outlet, one for a dip tube used to supply the loop pump sump tank, and one for a tube to transport the salt from the salt cleanup system to the storage tank. When the loop is in operation, the latter tubing is disconnected. The remaining tube is a spare. The storage tank is designed to operate at a temperature of up to 625°C (1160°F) at a pressure of 0.34 MPa (35 psig). American Society of Mechanical Engineers boiler and pressure vessel calculations for this tank are presented in Appendix A. The tank incorporates supports fabricated from 15 cm (6 in.) channel that sit on firebrick the same as those discussed for the pump sump tank below.

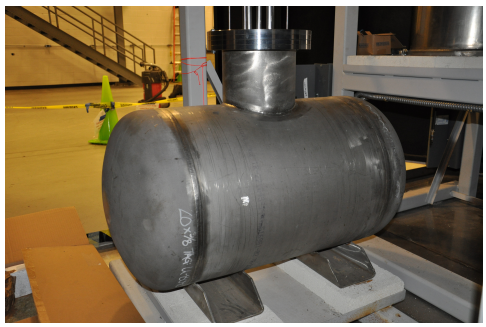

Fig. 5. Salt storage tank.

3.5 PUMP

A centrifugal sump-type pump with an overhung impeller is used, eliminating the need for salt-wetted seals and salt-lubricated bearings. The pump is capable of supplying 0.125 MPa head (18 psid) at 4.5 kg/s (3.57×10^4 lbm/h) flow rate. The pump volute and impeller are machined from Inconel 600; the pump is shown in Fig. 6. The pump is driven through a 1410 mm (55.5 in.) long, precision ground drive shaft that is 50 mm (2 in.) in diameter. A John Crane–type 2800 rotating shaft seal isolates the pump sump tank argon cover gas from the atmosphere. The pump shaft bearing housing uses two SKF 3210-2RS bearings that are located 318 mm (12.5 in.) apart. This overhangs the pump impeller by 902 mm (35.5 in.) from the centerline of the lower bearing to the top of the impeller. The pump shaft is connected to a 10 HP, 3600 RPM Brook Crompton motor through a Lovejoy flexible drive shaft (FVSLFS 1.5E). The flexible drive shaft is designed to accommodate 5 mm (0.2 in.) of axial movement and 4 mm (0.15 in.) of radial misalignment to allow axial expansion of the pump drive shaft and pump sump tank. The pump motor speed is controlled using a Lenze/AC Tech ESV752N04TFF variable frequency drive. The expected pump curve is shown in Fig. 7.

Fig. 6. Pump volute, impeller and top plate.

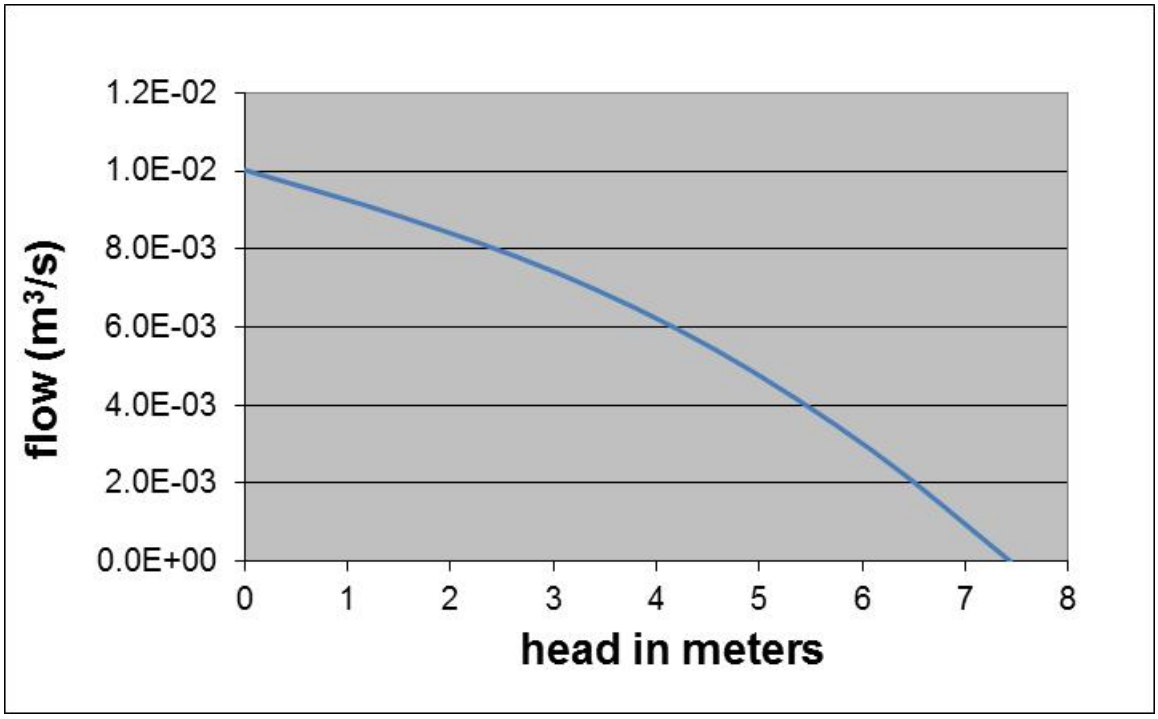

Fig. 7. Expected pump curve.

3.6 SUMP TANK

The loop design uses a sump that houses both the pump and a portion of the test section. The sump is sized sufficiently large to hold the entire loop salt inventory, providing a safe drain for all loop salt when needed. During operation the sump maintains a salt/argon interface. A pressurized argon gas system is used to move the salt from the sump tank into the test section and loop piping as well as maintain loop pressure at a few kilopascals. Normal tank operating pressure will be approximately 0.12 MPa (17 psia), but the tank was designed for 0.21 MPa (30 psia) using the finite element analysis code Solid Works (see Appendix B). The top flange of the tank includes a weldment for the pump shaft housing upon which the pump shaft seal and pump shaft bearing housings are mounted. It also includes the housing that contains the piston-type seals that are used as an argon seal for the SiC test section. These Stellite seals are manufactured by Precision Ring, Inc. The top flange also includes 12 penetrations for argon gas supply, salt transfer, and instrumentation that are designed similarly to those discussed in the surge tank section above. Two penetrations are for the argon gas inlet and outlet that are used to maintain the appropriate salt level in the loop. Two penetrations are used for heated thermocouple level indicators. One 38 mm (1.5 in.) diameter schedule 10 pipe extends to near the bottom of the tank and acts as a wave guide for a radar-based level detector. The slanted 38 mm (1.5 in.) diameter schedule 10 pipe, seen in Fig. 8, is designed to hold the pump exit pressure sensor. One 19 mm (3/4 in.) diameter penetration is used for installation of the transfer tube, used to transfer salt between the storage tank and pump sump. Two 50 mm (2 in.) diameter tubes are designed to accommodate two sight windows that allow visual observation of the salt in the sump tank. These tubes are topped with 304 stainless steel CF flanges 60 mm (2 3/8 in.) in diameter. The CF-type flanges are sealed using solid copper ring gaskets. The remaining three penetrations are used as spares. The design of the sump pump top flange accommodates a Parker C-type gas seal, which has a C-shaped cross section and compresses between the flange when loaded. Figure 8 shows a picture of the pump sump including the top flange. Figure 9 shows a picture of the Parker flange seal before installation.

Fig. 8. Sump tank and top flange.

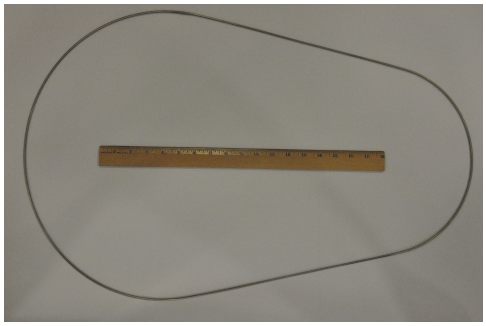

Fig. 9. Sump tank flange seal.

A 1.5 kW (5118 Btu/h), tubular-type heater manufactured by ABS Heating Elements is located on the bottom of the pump sump tank to assist in loop heat-up and ensure that the salt remains liquid while in the loop. The heater is serpentine in shape and attached to the bottom of the sump through stainless steel straps tack-welded to the bottom of the tank. Three type N thermocouples are also located on the bottom of the tank to assist in control of the tubular heating element. Figure 10 shows a schematic of the tubular heater located on the bottom of the pump sump tank. The tank sits on 10 cm thick (3.94 in.) firebrick (IFB 2300 U) manufactured by Morgan Thermal Ceramics that has a conductivity rating of 0.24 W/m°C at 540°C.

The pump volute and impeller, pump discharge piping, and transition to the test section are housed in the pump sump. These components are all attached to the pump sump top flange as seen in Fig. 11. The pump discharge piping is 50 mm (2 in.) schedule 40 pipe and includes a fitting to install the pump discharge pressure transducer. The fitting has a 25 mm (1 in.) National Pipe Thread (NPT) pipe thread that matches the end of the pressure transducer (Fig. 12). The pump discharge piping ends in a section that transitions the pipe discharge into the SiC test section. This section is cylindrical on the outside with an outside diameter (OD) just slightly smaller than the inside diameter (ID) of the SiC test section, allowing a slip fit between the test section and transition piece. This creates a leaky seal between the test section and transition piece and allows differential expansion between the metal portions of the pump sump tank and SiC test section. The transition section ID is conical, changing from 60 mm to 145 mm (2.375 in. to 5.72 in.) between the pump discharge and test section. It also includes the grid plate that holds the graphite pebbles and serves as the bottom of the pebble bed. A sketch of the transition piece is shown in Fig. 13. The pump discharge pipe and the transition piece are connected with a slip fit and a clamp system that also serves as a clamp to attach this piping to a hanger attached to the pump sump top flange (hidden in Fig. 11).

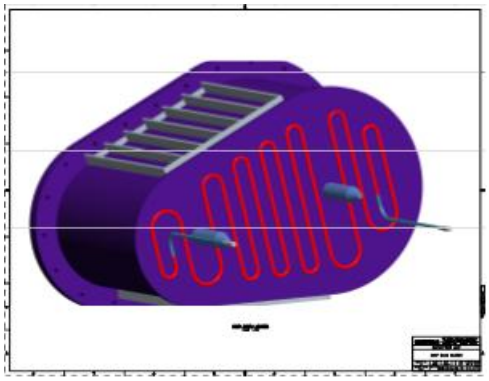

Fig. 10. Sump tank tubular heating element.

Fig. 11. Pump and top flange assembly.

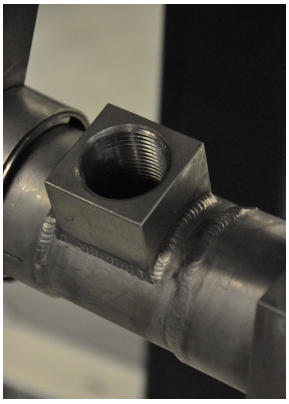

Fig. 12. Threaded fitting in pump discharge for pressure transducer.

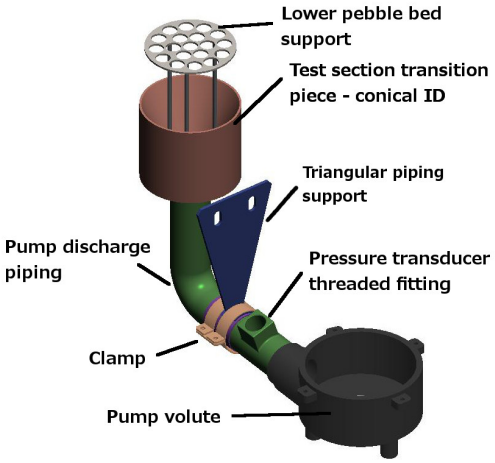

Fig. 13. Test section transition piece.

3.7 HEAT EXCHANGER

An air-to-salt heat exchanger is used to remove heat added by the inductively heated test section. The heat exchanger is a two-row finned tube design (seven tubes per row) with an outside surface area of 7.5 m^2 (80.7 ft^2) (including tubes). Cooling is supplied using a variable speed blower with a maximum volumetric flow of 2.8 m^3/s (355,972 ft^3/h). The heat exchanger tubes are 25 mm OD 1.65 mm wall (1 in. OD, 0.065 in. wall) alloy 600 tubing with 25 mm (1 in.) long 304 stainless steel fins 0.61 mm (0.024 in.) thick, approximately 97 fins/m (60 fins/ft). The fins are cut into 4 mm (0.156 in.) wide segments to facilitate wrapping around the tubes and attached to the tubing by tack welding. The finned tubes were manufactured by Class Ten Industries and cut to appropriate length.

The straight finned tubes are attached to tube sheets at either end that are 3 mm (1/8 in.) thick and terminate in header tanks that are tapered to allow all salt to drain and all gas to be eliminated when filling with salt. A 1 kW (3412 Btu/h), tubular-type heater manufactured by ABS Heating Elements is located on

each of the heat exchanger tanks to facilitate heat-up prior to salt filling. A picture of the heat exchanger is shown in Fig. 14. The heat exchanger assembly is housed in an insulated shell that supports its weight. The shell is located within air ducting that allows the heat exchanger to move in all directions to accommodate thermal expansion. The duct system incorporates insulated doors on the front and rear faces of the heat exchanger that allow heat-up prior to filling with salt. The doors can be raised and lowered by a cable system, allowing the heat exchanger face opening to be varied depending on the heat load. Two 0.85 kW (2900 Btu/h)tubular heater assemblies fabricated by ABS Heating Elements are located at the front and rear faces of the heat exchanger to assist in heating the loop.

Fig. 14. Air-cooled heat exchanger.

The heat exchanger assembly (heat exchanger and shell) is suspended within the ductwork using two spring hangers (Anvil International – Type C), allowing the heat exchanger to move in all directions due to thermal expansion. The hangers are attached to the top of the heat exchanger shell through two lugs that extend through the ductwork and are attached to the hangers with threaded rod. The spring hangers are attached to the loop framework.

All of the tanks (storage, sump, and surge) as well as the heat exchanger were pneumatically pressure tested individually and then helium leak checked. The test pressures are shown in Table 2, along with the relief pressures for each tank. A stress calculation for the piping is presented in Appendix C.

Table 2. Loop tank and relief pressures

Tank	Test pressure MPa (psig)	Relief pressure MPa (psig)
Surge	0.92 (119)	0.19 (15)
Pump sump	0.58 (69)	0.31 (30)
Storage tank	0.92 (119)	0.34 (35)
Heat exchanger	0.45 (50)	—

3.8 INSTRUMENTATION

Loop instrumentation includes salt temperature and pressure measurements, sump and surge salt levels, as well as measurement of the salt flow rate. A process and instrumentation diagram of the salt loop is presented in Fig. 15. The instrumentation and control system is based on the Rockwell ControlLogix programmable logic controller (PLC) platform using ControlLogix inputs and outputs and Flex I/O inputs and outputs as shown in Fig. 16. The software RSView is used for the human-machine interface and data acquisition functions.

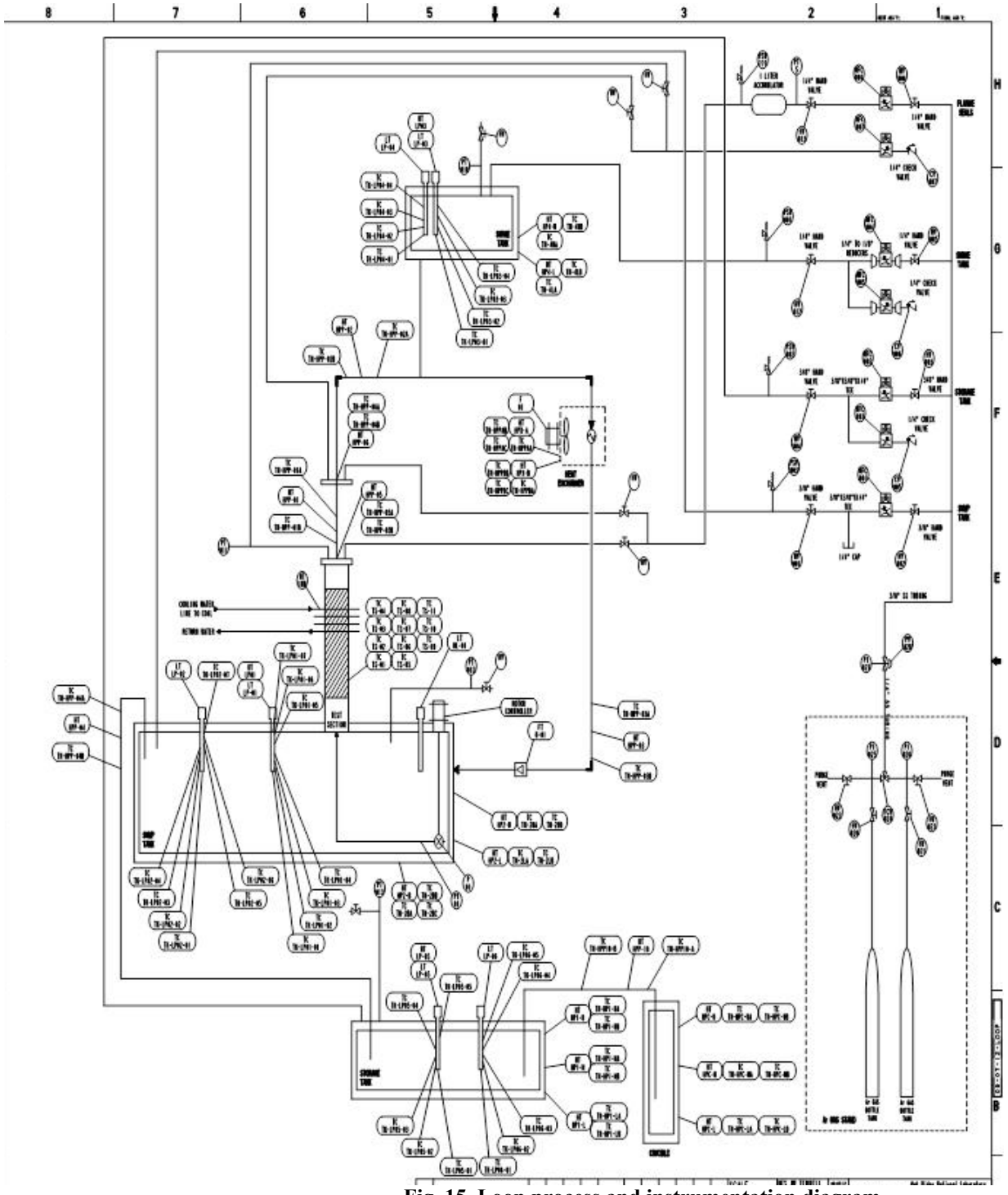

Fig. 15. Loop process and instrumentation diagram.

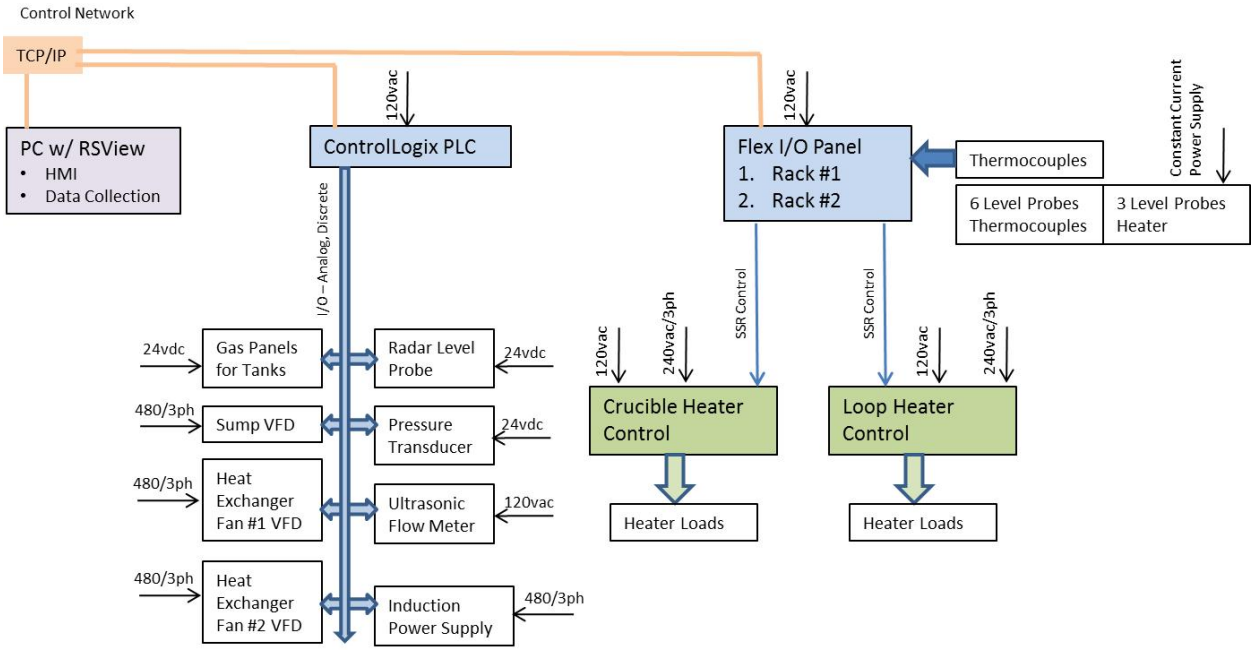

Fig. 16. Instrumentation and control system.

3.8.1 Temperature

Temperature measurements inside the pebble bed include salt temperatures and pebble temperature measurements made by inserting thermocouples through the test section flange and into the bed. Eight 0.5 mm (0.020 in.) diameter nickel-sheathed type S thermocouples that are 1200 mm (48 in.) long are threaded into the test section through the top flange and sealed using a Conax fitting with boron nitride compression material. Delta-M Corporation manufactured these thermocouples. The type S thermocouples (platinum – platinum/rhodium) used in the bed are minimally impacted by the inductive field, and testing in separate experiments has confirmed this conclusion. Bed thermocouples are located at the test section inlet and outlet to measure salt temperatures. Two thermocouples are located at the inlet and outlet by attaching them to the bed inlet and outlet grids. Two thermocouples are fixed at the centerline of two pebbles by first threading them through a hole drilled in the pebble and then turning them into a hole bored into the center of the pebble (Fig. 17). Two thermocouples are located near the instrumented pebbles in the salt space by first threading them through an uninstrumented pebble and then bending them into the salt space. The bed thermocouples were carefully placed in the bed as it was being built, and the remainder of the bed was built around them.

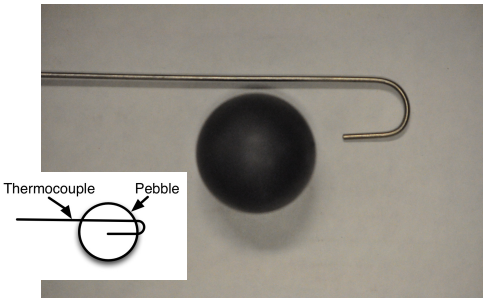

Fig. 17. Graphite pebble with thermocouple.

Thermocouples are also placed at various positions around the loop to aid in trace heating, which is designed to ensure that all of the loop is above the salt melt temperature before filling with salt and that the salt can never freeze during operation. These type N (nickel-chromium-silicon/nickel-silicon) thermocouples are attached to the piping and the heat exchanger using thermocouple wells, integral with the heating blankets, and attached to loop flanges to confirm loop component temperatures. A summary of thermocouple numbers and location is shown in Table 3.

Table 3. Loop thermocouple count and type

T/C location	Number of T/Cs	Type
Pebble bed	8	S
TS to HX piping	2	N
HX to pump ump piping	2	N
HX	6 (inlet and outlet)	N
Pump sump heating blanket	7	N
Surge tank heating blanket	4	N
Storage tank heating blanket	12	N
HX air cooling	2 (1 inlet, 1 outlet)	K
TS top flange	2	N
Surge tank piping flange	2	N

HX = heat exchanger
T/C = thermocouple
TS = test section

3.8.2 Salt Flow Rate

Salt flow rate is measured using an ultrasonic flow meter manufactured by Flexim, Inc. The Flexim WaveInjector meter was specifically designed to operate at a loop temperature of 700°C. The flow meter wave guides were designed so that the piezoelectric transducer system (PIC 255) remained at a safe operating temperature (< 350°C) while still providing sufficient coupling to maintain accuracy levels. The 304 stainless steel wave guides and piezoelectric transducer system were tested by using a heated and insulated 25 mm (1 in.) schedule 40 pipe internally heated with an electrical heater to provide a 700°C boundary condition for the blades. Both thermocouple measurements and infrared imaging confirmed that the transducer mounting location would remain below the acceptable temperature limit. The blades (stepped plates in Fig. 18) are mounted to the 25 mm (1 in.) schedule 40 piping using a series of clamps. The two blades are mounted 180° apart on 3 mm (0.12 in.) wide, 328 mm (12 in.) long flats that are machined onto the piping. The flats were machined onto both the piping leading from the test section to the heat exchanger as well as the piping from the heat exchanger to the sump tank, allowing the flow meter to be placed on either leg of the pipe. Twenty pipe diameters were maintained between the elbows of these pipes and the flow meter entrance and at least five diameters downstream of the flow meter to minimize the effect of secondary flow on the flow meter readings. Armored cable was used between the piezoelectric transducer and the Flexim electronics that were located outside of the walk-in hood. (The armored cable was designed to minimize noise induced by operation of the inductive power supply.) The Flexim electronics provide an interface with the Allen-Bradley data acquisition system and allow recording of the salt flow rate. The manufacturer's expected flow rate error (one standard deviation) is approximately 5.5%. A picture of the flow meter is shown Fig. 18.

3.8.3 Pressure Measurement

Gas pressures are measured for the three tanks that are included in the loop design: storage tank, pump sump, and surge tank. All of these measurements are taken using 0–0.41 MPa (0–60 psi) Omega PX209-060GI pressure transducers. These transducers are located on each tank through a 6.35 mm (1/4 inch) diameter stainless steel line that keeps the transducer temperature sufficiently low. The transducers provide a 4–20 mA output to the loop data acquisition system. The manufacturer's estimated accuracy for these transducers is 0.25% full-scale reading or approximately 1×10^{-3} MPa (0.15 psi).

The pump salt discharge pressure is measured using a 0–0.34 MPa (0–50 psi) GP-50 NaK capillary isolated pressure transmitter. The transmitter has a manufacturer's estimated accuracy of 0.2% full scale and has thermal compensation up to 700°C. The design includes a nickel 201 diaphragm with the remainder of salt-wetted parts made of alloy 600. Figure 19 shows a picture of the salt pressure transducer with the diaphragm end located to the left of the figure. This transmitter is located in the pump discharge line, between the pump and the test section transition piece (see Fig. 13). It connects to the pump discharge line using a 25 mm (1 in.) NPT fitting. A close-up of the diaphragm end of the transmitter with

the NPT fitting is shown in Fig. 20. This end of the transmitter is threaded, and the transmitter extends through the pump sump top flange via a 38 mm (1.5 in.) schedule 40 tube that allows the top of the transmitter to be sealed against the argon cover gas in the sump tank using a Swagelock compression fitting and Teflon seal. A NaK-filled capillary is used to transfer the pressure signal from the diaphragm to the transducer system, which must operate at significantly lower temperatures than the salt. The electronics (right side of Fig. 19) are connected to the transducer through flexible electronic leads. The transmitter includes a 4–20 mA output that allows communication with the data acquisition system.

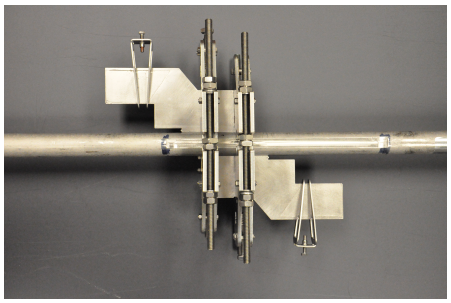

Fig. 18. Flexim ultrasonic flow meter.

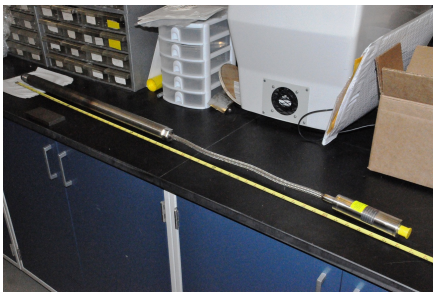

Fig. 19. Salt pressure transmitter (diaphragm on left of figure and electronics on right).

Fig. 20. Threaded end of pressure transducer and diaphragm.

3.8.4 Trace Heating

Because FLiNaK salt solidifies at 454°C, the loop is designed so that all components that are in contact with salt can be heated above the FLiNaK melt temperature. The tanks and loop piping are heated using a combination of heating tapes and heating blankets along with flexible insulation. All three loop tanks are heated using HTS/Amptek heating blankets. Each blanket consists of a combination of heaters, 10.2 cm (4 in.) of insulation, and thermocouples to monitor system temperatures. These blankets are capable of operating up to 750°C. All of the blankets have zones of heat that allow power to be applied to the top portion of the tanks before applying power to the bottom to allow rethawing of the salt in the tank in the unlikely event that salt freezing occurs. (The storage tank is specifically designed for this.) Table 4 shows each blanket, the number of heating zones, and the maximum power that can be applied to each zone. The insulation thickness is designed such that the outer surface temperature of the blankets while operating will stay below 60°C for personnel protection. The flanges on all of the tanks are covered with 10.2 cm (4 in.) of insulation (unheated), while the storage tank end caps are also covered with insulation but are unheated. A picture of the heating blanket on the pump sump tank in Fig. 21 shows the imbedded thermocouples and heaters as they exit the blanket. Other sections of the loop such as piping and flanges are heated using HTS/Amptek heating tapes and Zircar insulation wrap. These sections use separate type

N thermocouples located on these components for temperature control. Approximately 7.6 cm (3 in.) of Zircar RSMAT-3000 were used for these piping components. RSMAT-3000 has a thermal conductivity of 0.13 W/mK at 760°C and can operate at temperatures up to 1650°C. The test section was also heated and similarly insulated. Above and below the inductive coil, 7.6 cm (3 in.) of insulation were used, and between the coil and SiC flow tube, 2.54 cm (1 in.) of insulation were used. Inventories of heating tapes and tubular heating elements are presented in Tables 5 and 6, respectively. The control and circuit protection for each heating zone is performed using ground fault interrupter circuit breakers, solid-state relays, and PLC control. The loop heater control enclosure is shown in Fig. 22.

Table 4. Heater blanket design

Tank	Number of zones	Power, W (Btu/h)	
Surge	2	Upper zone	528 (1,800)
		Lower zone	528 (1,800)
Pump sump	3	Upper zone	1,860 (6,350)
		Lower zone	1,860 (6,350)
		Bottom zone	2,000 (6,825)
Storage	3	Upper zone	4,000 (13,650)
		Middle zone	2,000 (6,825)
		Lower zone	2,000 (6,825)

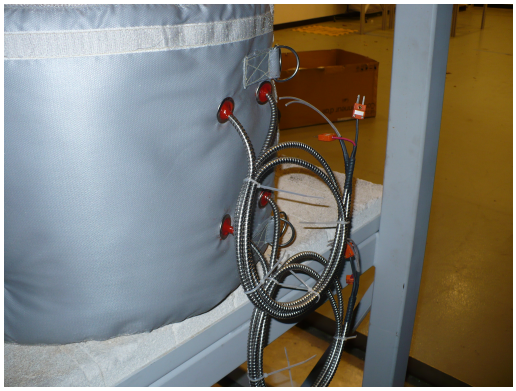

Fig. 21. Sump tank heater blanket showing electrical and thermocouple leads.

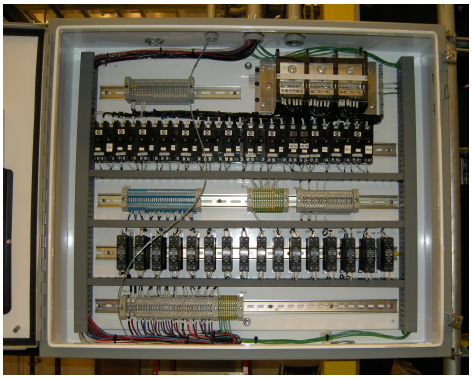

Fig. 22. Loop heater control enclosure.

Table 5. Heating tape location and rated power

Location	Power, W (Btu/h)
Test section flange	500 (1706)
Test section to surge tank pipe	1000 (3412)
Surge tank piping flange	400 (1365)
Surge tank to heat exchanger	500 (1706)
Heat exchanger to pump sump	1000 (3412)
Lower test section	500 (1706)
Upper test section	500 (1706)

Table 6. Tubular heater locations and rated power

Location	Power, W (Btu/h)
Pump sump bottom	1500 (5118)
Air HX – air inlet	750 (2559)
Air HX – air outlet	750 (2559)
Air HX – bottom manifold	1000 (3412)
Air HX – top manifold	1000 (3412)

HX = heat exchanger

3.8.5 Pressure and Level Control

Four cover gas control systems are used to control pressure and salt level in the loop and also provide the inert gas buffer in the space between the Flexitallic gaskets (spiral-wound Ni and grafoil) and gas seal system that are used in both the test section flange and the test-section-to-heat-exchanger piping. Each system consists of two Porter mass flow controllers, an Omega pressure transducer (discussed above), a relief valve to prevent overpressurization of the loop, and a check valve to prevent air from entering the argon gas system. Figure 23shows a picture of select components of the gas supply systems. The inlet line for each panel includes an isolation valve to isolate the gas supply bottles from the loop to allow component change out. One gas system is used to supply the storage tank, one the pump sump tank, one the surge tank, and one the flange seals. Each is similarly designed but with differing rated flow and pressure and relief values depending on the tank (or flanges) being serviced. Table 7 shows the system ratings of each of the cover gas control systems.

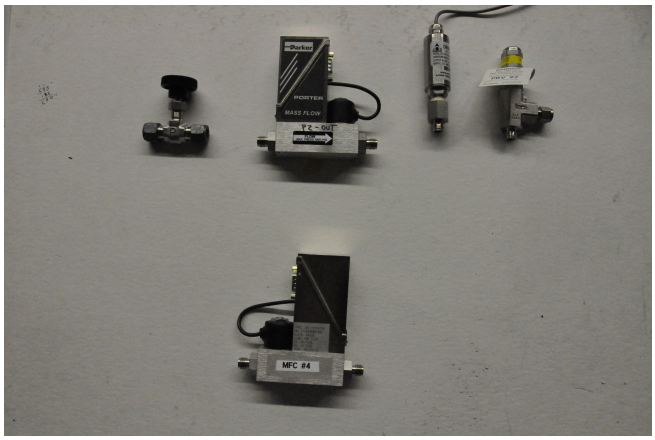

Fig. 23. Components used to control pressure and flow in the loop.

Table 7. Cover gas control system ratings

System	Pressure transducer, MPa (psia)	Supply mass flow control, L/m (ft^3/h)	Let-down mass flow control, L/m (ft^3/h)	Pressure relief, MPa (psig)
Storage tank	0–0.41 (0–60)	0–10 (0–21)	0–5 (0–10.5)	0.19 (15)
Sump tank	0–0.41 (0–60)	0–100 (0–212)	0–0.2 (0–0.42)	0.31 (30)
Surge tank	0–0.41 (0–60)	0–0.2 (0–0.42)	0–0.2 (0–0.42)	0.19 (15)
Flanges	0–0.41 (0–60)	0–0.2 (0–0.42)	0–0.2 (0–0.42)	0.38 (40)

The salt level in each tank is monitored by heated thermocouple level detectors. Each tank has two sets of heated thermocouple arrays with discrete level measurements. Figure 24 shows the thermocouple location for each set of level detectors. Only one of the arrays is heated during operation. (Both are designed to be heated as a way of providing a spare for each tank.) Each detector is heated along its length, and thermocouples are located at discrete points along it. For those thermocouples located beneath the liquid surface, the measured temperature is low because the heat transfer from the detector surface to the liquid is high. For thermocouples located above the liquid surface, in the argon cover gas, the heat transfer from the detector is poor, and the measured temperatures are higher. The level is detected by reading the differences in temperatures between thermocouples located in the argon and liquid regions. The second array in each tank is unheated and is used to correct for temperature variations in the liquid and vapor that may be present in the tank. An Omhart Vega, VEGAPULS 62, radar-based level detector is located on the pump sump tank. This detector is threaded into an alloy 600 wave guide that reaches to within approximately 1.8 cm (0.7 in.) of the tank bottom and extends above the pump sump tank flange approximately 61 cm (24 in.) to ensure that the electronics remain cool. The detector, shown in Fig. 25, provides a continuous salt level measurement with a manufacturer's rated accuracy of approximately 1 mm (0.039 in.).

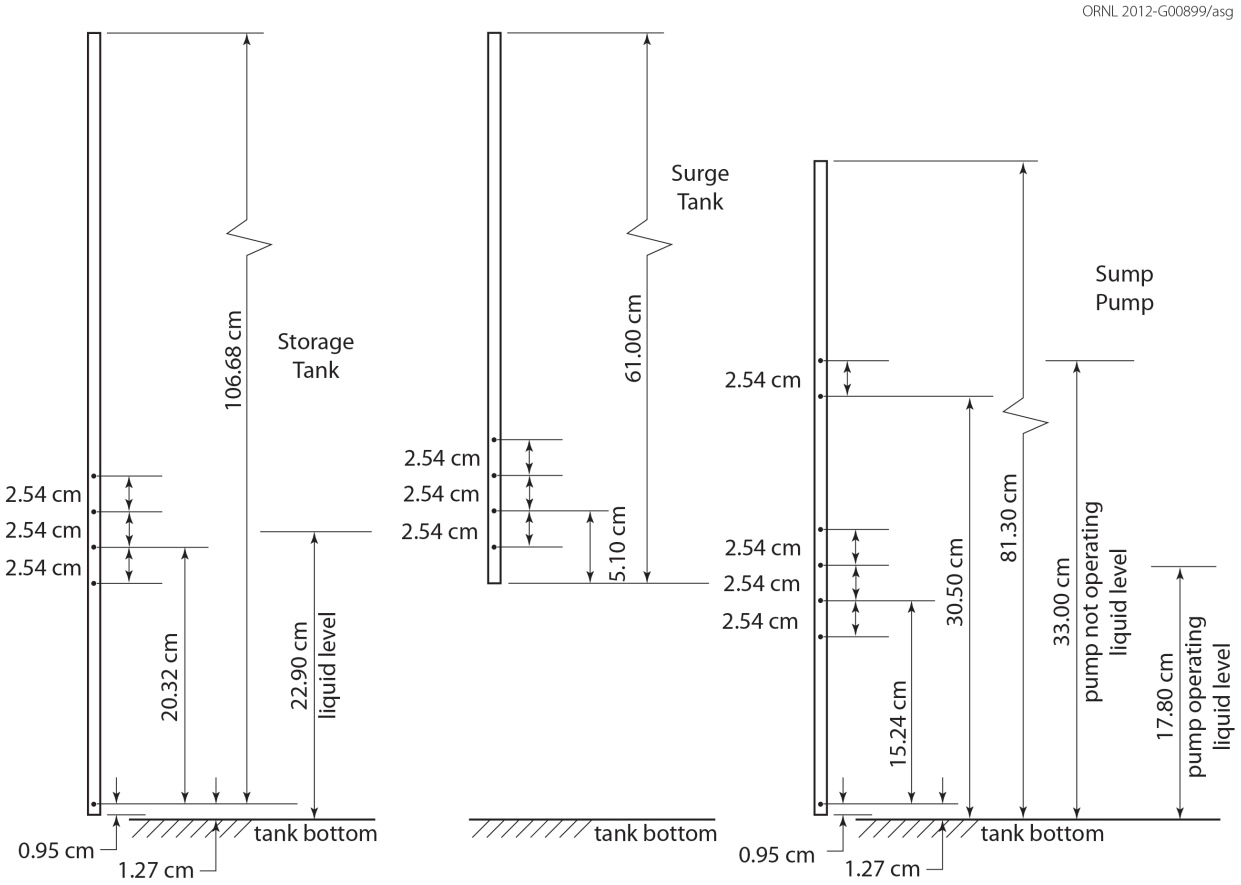

Fig. 24. Level detector thermocouple location.

3.9 TEST SECTION

A Bone-Frontier Evolution 5 inductive heating system provides volumetric heating in the pebble bed. The test section design uses a SiC flow channel and solid graphite pebbles as the susceptor. The SiC flow channel is 15 cm ID and has a 6.35 mm wall thickness. The 3 cm (1.18 in.) diameter pebbles are fixed in the flow channel using grids that extend from the flow diffuser at the entrance to the test section and above from the Inconel top flange. Approximately 600 pebbles form the bed. A bed height of 24 cm (9.45 in.) is used to condition the flow into the 24 cm (9.45 in.) long heated region. An additional 24 cm (9.45 in.) of bed height at the top of the heated bed region separates any metallic structures from the inductive heater. Figure 26 shows a diagram of the test channel, and Fig. 27 shows a picture of the channel before installation. The top of the SiC flow channel incorporates a flange that interfaces with the Inconel top flange using a Flexitallic gasket. This gasket is a spiral-wound design using alternating spirals of grafoil and nickel. A secondary C-type gas seal (Parker) surrounding the Flexitallic gasket is used to provide a sealed inert gas space between the Flexitallic and C seal for leak detection and to ensure that no air can get into the loop.

Fig. 25. Ohmart Vega radar-based level detector.

A piston-ring-type gas seal is used between the SiC test section and the top of the pump sump tank. This seal uses three split-seal rings that are installed in circumferential grooves machined in a collar welded to the top of the pump sump. These rings compress around the circumference of the test section, preventing gas leakage between the collar and test section but allowing axial expansion of both the test section and sump tank. Three, three-ring sets are used to maintain the gas seal. The rings were fabricated by Precision Ring, Inc. One three-ring set is shown in Fig. 28.

Fig. 26. Schematic of SiC test section.

Fig. 27. Silicon carbide flow tube test section as manufactured.

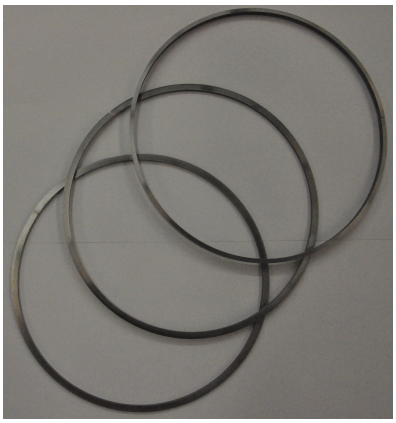

Fig. 28. Piston-ring seal use for test section.

3.10 INDUCTION POWER SUPPLY

A Bone-Frontier Evolution 5 inductive power supply operating at a frequency of 30 kHz is used to provide 200 kW to the pebbles. Inductive heating provides a method of accurately simulating the internal heat generation in the fuel pebbles without any direct electrical connections. There is approximately 90% coupling to the pebbles and test section. This includes 2–5% to the SiC flow tube and 7–14% to the FLiNaK salt. Two coil designs have been fabricated to evaluate the power supply coupling capability. One coil has five turns (Fig. 29), and one a total of six. Figure 30 shows the power supply system used for the FLiNaK test loop.

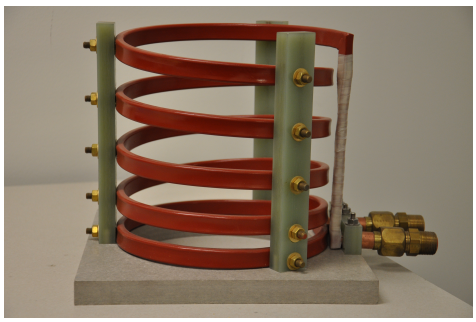

Fig. 29. Induction heating coil.

Fig. 30. Inductive power supply.

3.11 LOOP STARTUP, OPERATION, AND SHUTDOWN

When not in use, the loop is inerted using a high-purity argon cover gas. The loop startup process requires that the salt storage tank and stored salt temperature be raised above the melt temperature. The storage tank temperature is increased until the salt is melted and then raised to about 600°C (1100°F). The storage tank heater blanket system is designed to allow heat to be separately applied in three vertical zones. This configuration ensures that the frozen salt can be heated from the top down and that no melt region can be trapped by frozen salt, potentially overstressing the storage tank (FLiNaK expands when melting). The remainder of the loop is then held at a temperature of about 600°C (1100°F) before transferring the salt from the storage tank to the sump tank. To effect this transfer, once the salt is melted and the storage tank and loop temperatures stabilized at 600°C (1100°F), the pressure in the storage tank is sufficiently raised using the storage tank argon pressure control system to push the salt through the inverted U-bend transfer tube (see Fig. 2) and into the sump tank, which is maintained at a lower pressure than the storage tank. When the transfer is complete (detected by examining pressures and salt levels in the two tanks), the salt is then raised into the remainder of the loop by pressurizing the sump tank through either the sump tank argon pressure control system or the storage tank argon pressure control system, or both. Pressure is increased until the salt level reaches about the middle of the surge tank (detected using surge tank level instruments). At this point the loop is filled with salt, and the loop operating pressure is adjusted through the surge tank argon pressure control system. Flow through the loop is then started with the pump, power to the test section applied through the inductive heating system, the heat exchanger trimmed to allow appropriate heat rejection, and testing initiated.

Shutdown is essentially the reverse of startup. The heat exchanger is shut off, the inductive power is turned off, and the pump is stopped. The pressure in the sump tank is then reduced, lowering the salt from the loop piping into the sump tank. The pressure in the sump tank (and the remainder of the loop) is raised, forcing the salt through the U-bend tube between the sump tank and storage tank and into the storage tank. Once all of the salt is transferred, the loop and storage tank are reduced in temperature, and the salt allowed to freeze in the storage tank.

4. LOOP OPERATING CONDITIONS

4.1 LOOP DESIGN CONSIDERATIONS

A series of calculations was performed during the design of the loop that was used to establish the loop operating conditions, size, etc. The focus of the loop design was on establishing thermal/fluid characteristics in the pebble bed so that the PB-AHTR conditions could be simulated. An additional constraint on the loop design was imposed by imposing loop cost considerations; this limited the scale of the system. Several characteristics of the PB-AHTR core were considered in the design process. Matching the pebble Reynolds ensures that heat transfer and fluid conditions in the experimental system match those of the reactor:

$$Re_P = \rho\, v_s\, D_p/\mu,$$

where

ρ = salt density,
v_s = bed superficial velocity,
D_p = pebble diameter, and
μ = salt viscosity.

The pebble diameter for the present PB-AHTR design is 3 cm (1.18 in.), and this is the diameter of the pebbles used in the experiment. The reactor operates at 700°C (1290°F), and the core pebble bed superficial velocity is 0.35 cm/s (0.0115 ft/s). The fluid used in the reactor is FLiBe. This results in a reactor pebble Reynolds number of

$$Re_{P,R} = 3100.$$

Based on a variety of tradeoffs, mostly related to the size of the loop and loop components such as the pump and their impact on loop construction costs, it was decided that the pebble Reynolds number for the experiment should be above the critical value to ensure fully turbulent flow (2000) [13] but not require that Re_p exactly match that of the reactor design. Ultimately, after making these tradeoffs, the pebble Reynolds number for the experiment is $Re_p = 2600$.

Pebble beds have a gradient of liquid fraction near the bounding wall because the presence of a wall limits the degree of pebble packing that can occur. In the case of the reactor, the bounding wall is the 20 cm (7.8 in.) flow channel. The nondimensional length scale (D*) used in evaluating the effect of the bounding wall is the bed-to-pebble diameter (D_b/D_p):

$$D^* = D_b/D_p,$$

where

D_b = bed diameter and
D_p = pebble diameter.

Various studies[7,8] have shown that only when D* is over approximately 25 does the wall effect on the liquid fraction become unimportant at the center of the bed. D* for the reactor design is approximately 6.7, so there is significant wall impact on the liquid fraction throughout the bed. Both because the PB-AHTR did not have a bed diameter sufficient to achieve D* of 25 and in order to minimize the flow required to the bed while maintaining an appropriate pebble Reynolds number, a bed diameter of 15 cm (5.9 in.) was selected for the experiment.

It was desirable to ensure that the flow within the bed became fully developed before it entered the test section. “Fully developed” in this context means that the fluid velocity profile across the bed is no longer axially changing as it enters the heating zone. In reality, the geometry of the bed, because of random pebble packing, does not ever become fully developed. A series of computational fluid dynamics studies using the FLUENT code was used to evaluate the velocity profiles within the bed. The objective of these studies was to determine how many pebble rows were needed before the heated section of the bed to establish a fully developed flow pattern. These calculations indicated that 4–6 pebble diameters (or layers) were needed to achieve a nearly fully developed velocity profile across the bed. The final design includes eight pebble layers (24 cm [9.45 in.]) before the heated section to ensure that the flow is fully developed. The inductively heated region of the bed is 24 cm (9.45 in.) in length, and another 24 cm (9.45 in.) pebble region after the heated region keeps any metallic components at a sufficient distance to eliminate any possibility of heating due to the inductive field. These considerations established the required pebble bed length of 0.75 m (29.5 in.) used in the experiment.

The experimental salt mass flow rate requirement is established by the bed diameter and the pebble Reynolds number. These combine to set a required loop mass flow rate of 4.5 kg/s (3.57×10^4 lbm/h). The loop pressure drop at this flow rate is approximately 0.125 MPa (18 psid).

4.2 LOOP THERMAL/FLUID CONDITIONS

A series of parametric calculations was performed during the loop design process to evaluate potential design options. These calculations included thermal and pressure-drop calculations in the loop. Pressure drops in the piping, heat exchanger, and pebble bed were calculated separately along with the heat transfer from the pebbles within the bed. A summary of calculation results is presented in Table 6 assuming about 150 kW (5.12×10^6 Btu/h) into the pebbles from the inductive power supply and a salt flow rate of 4.5 kg/s (3.57×10^4 lbm/h). Table 8 references the schematic and loop locations shown in Fig. 31. Details of how the numbers in Table 8 were generated are presented in Appendix D.

Table 8. Loop pressure drop and temperature characteristics

Location	Pressure, MPa (psia)	Temperature, °C (°F)
Pump discharge	0.307 (44.5)	680 (1256)
Test section outlet	0.252 (36.5)	700 (1292)
Surge tank liquid level	0.205 (29.7)	700 (1292)
Heat exchanger inlet	0.207 (30.0)	700 (1292)
Heat exchanger outlet	0.189 (27.4)	680 (1256)
Pump suction	0.157 (22.8)	680 (1256)
Sump liquid level	0.151 (21.9)	680 (1256)

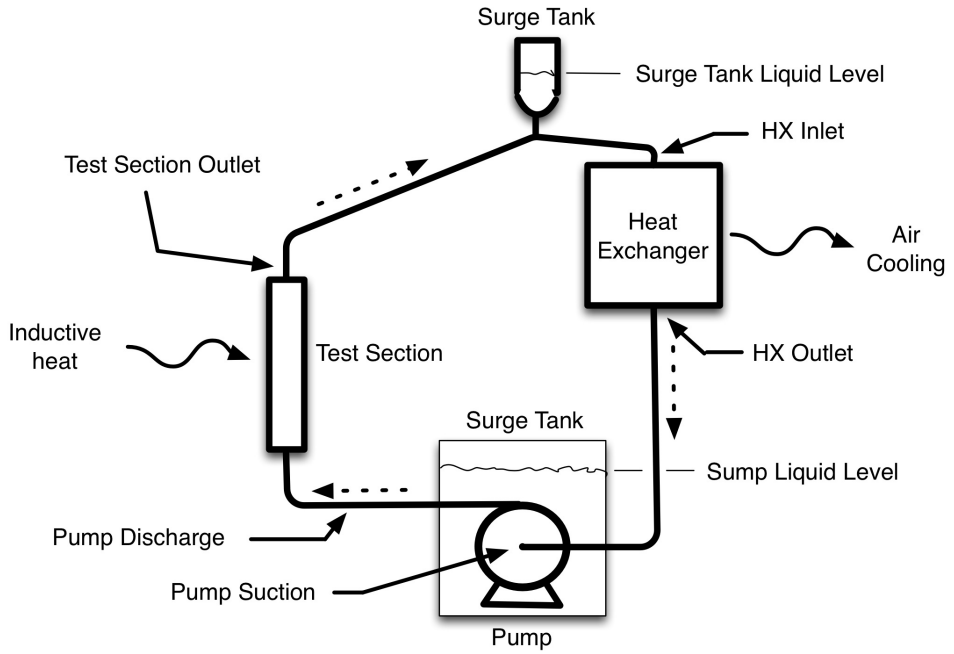

Fig. 31. Loop schematic diagram.

With a pebble power of 1285 W (4385 Btu/h) and the loop operating at a flow rate of 4.5 kg/s (3.57×10^4 lbm/h), the temperature rise from the salt to the surface of the pebble is approximately 53°C (95°F).

The loop operating characteristic and the pump curve at 3600 rpm are presented in Fig. 32, showing the design operating point. Loop flow rate is reduced by reducing the pump speed, essentially moving the

pump curve from the one in the figure down and to the left as the pump speed reduces, allowing multiple points on the loop operating curve to be evaluated.

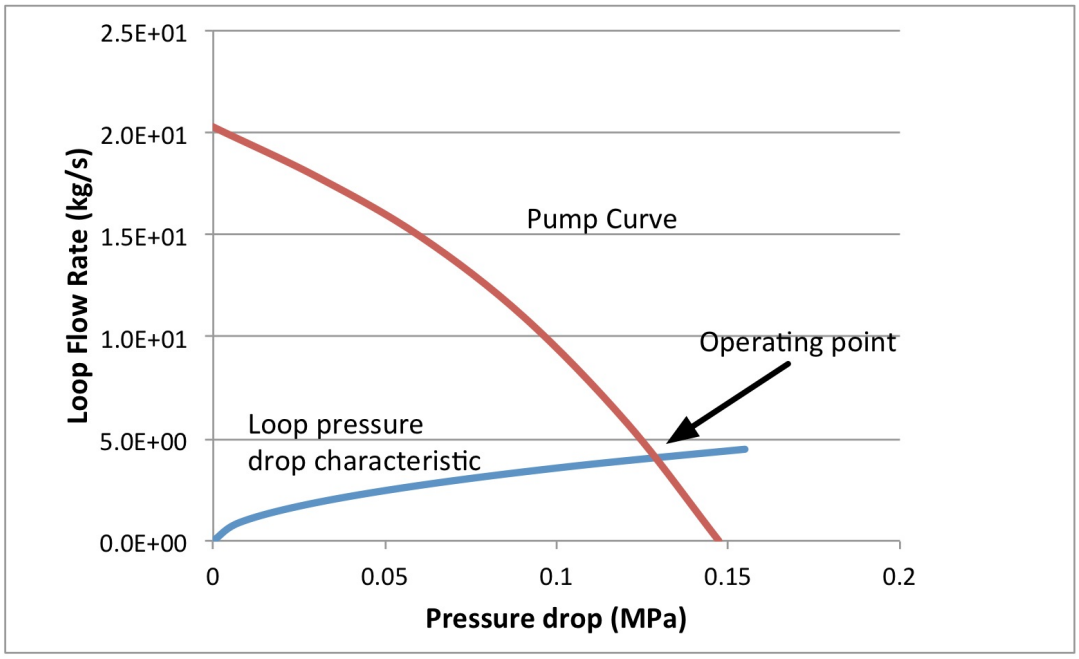

Fig. 32. Loop characteristic and pump curve.

4.3 INDUCTIVE HEATING

The inductive heater is designed to apply a maximum of 1285 W/pebble (peak) (4385 Btu/h), the same as the PB-AHTR reactor. The inductive heating system does produce a radial field distribution across the bed. There is about a 4% peak in the field at the edge of the bed and a 2% depression at the center of the bed relative to the average radical H-field (Fig. 33).

Similarly, there is also an axial variation in the inductively induced field distribution in the bed. This distribution varies with a 15% peak-to-average value at the center of the coil to a 23% depression at the top and bottom of the coil. Figure 34 shows the predicted axial variation within the bed.

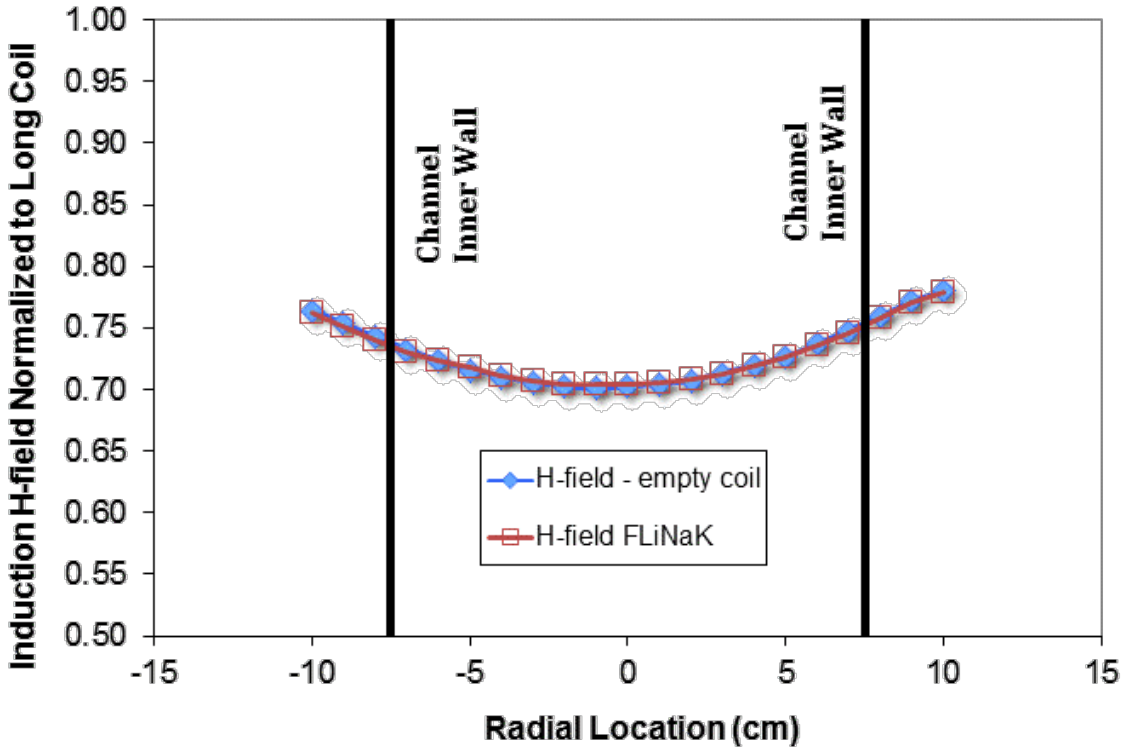

Fig. 33. Radial distribution of induction H-field at 30 kHz with and without FLiNak salt (24 cm [9.45 in.] diameter coil 24 cm [9.45 in.] long).

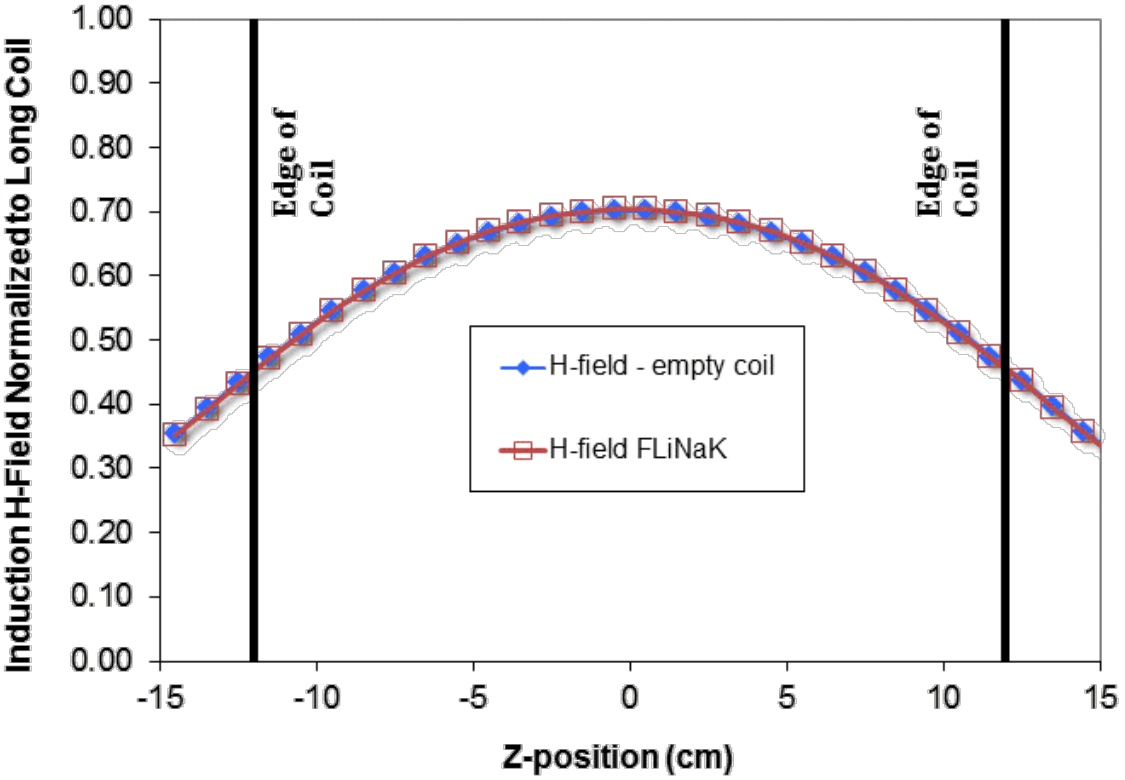

Fig. 34. Axial Distribution of Induction H-field at 30 kHz for a 24 cm diameter coil 24 cm long.

5. REFERENCES

1. P. Bardet et al., "Design, Analysis and Development of the Modular PB-AHTR,"*International Congress on Advances in Nuclear Power Plants (ICAPP 2009)*, Curran Associates, NY, May 2009, pp. 161–178.
2. S.R. Greene, "SMAHTR – A Concept for a Small Advanced High Temperature Reactor," *Proceedings of HTR-10*, Prague, Czech Republic, October 18–20, 2010.
3. V. Varma et al. "AHTR Mechanical, Structural, and Neutronic Preconceptual Design," ORNL/TM-2012/320, Oak Ridge National Laboratory, Oak Ridge, TN, September 2012.
4. N. Wakao, *Heat and Mass Transfer in Packed Beds*, Gorden and Breach, Science Publishers, Inc., New York, 1982.
5. N. Kolev, *Packed Bed Columns: For Absorption, Desorption, Rectification, and Direct Heat Transfer*, Elsevier, The Netherlands, 2006.
6. S.S. Yee and K. Kamiuto, "Combined Forced-Convective and Radiative Heat Transfer in Cylindrical Packed Beds with Constant Wall Temperatures," *Journal of Porous Media* **8**, 481–492 (2005).
7. B.P. Singh and M. Kaviany, "Modeling of Radiative Heat Transfer in Packed Beds," *International Journal of Heat and Mass Transfer* **35**, 1397–1405 (1992).
8. K. Ridgway and J. Tarbuck, "Voidage Fluctuations in Randomly-Packed Beds of Spheres Adjacent to a Containing Wall," *Chemical Engineering Science* **23**, 1147–1155 (1968).
9. J.D. McWhirter, M.E. Crawford, and D.E. Klein, "Wall Region Porosity Distributions for Packed Beds of Uniform Spheres with Modified and Unmodified Walls," *Transport in Porous Media* **27**, 99–118 (1997).
10. V.S. Travkin, K. Hu, and I. Catton, "Turbulent Kinetic Energy and Dissipation Rate Equation Models for Momentum Transport in Porous Media," *Proceedings of the 3rd ASME/JSME Joint Fluids Engineering Conference*, American Society of Mechanical Engineers, 1999, pp. 1–7.
11. M.H.J. Pedras and M.J.S. de Lemos, "On the Definition of Turbulent Kinetic Energy for Flow in Porous Media," *International Communications in Heat and Mass Transfer* **27**, 211–220 (2000).
12. H. F. Nielsen, "The Sana-I Experiment for Self-Operating Removal of Afterheat," IAEA Research Coordination Meeting "Heat Transport and Afterheat Removal for Gas-Cooled Reactors Under Accident Conditions," Vienna, November 17–19, 1993.
13. M. Rhodes, *Introduction to Particle Technology*, Wiley, England, 1989.

APPENDIX A. STORAGE TANK PRESSURE CALCULATIONS

APPENDIX A. STORAGE TANK PRESSURE CALCULATIONS

Pressure calculations were performed for the storage tank, sump tank, and piping system. The surge tank will operate at pressures below 15 psig, and specific calculations for this tank were not performed.

Design Summary Sheet

Molten Salt Loop Storage Tank
Designed per
ASME Section VIII, Division 1 (2010 Edition, 2011 Addenda)

1. The attached engineering calculations support the design of a pressure vessel designated as a Molten Salt Loop Storage Tank, as depicted in UT-Battelle, LLC Dwg. No.: MSSK040610-009, Rev. 0. This design complies with the rules of ASME Section VIII, Division 1 (2010 Edition, 2011 Addenda). Only loads resulting from internal pressure were considered in the design of the vessel. No external piping support or reaction loads have been identified or considered in the design. No internal or external corrosion allowances have been specified.

2. The vessel is designed for a maximum allowable working pressure (MAWP) of 35 psig @ 1160°F and a maximum allowable external working pressure (MAEWP) of 15 psig (full vacuum) at 1160°F. An acceptable minimum design metal temperature (MDMT) of -20°F @ 35 psig (and full vacuum) is acceptable without requiring toughness testing per UHA-51(d)(1), UHA-51(e)(2)(b) and UNF-65.

3. The engineering calculations demonstrate the selected materials and thicknesses are acceptable for the design conditions. The shell, heads and nozzle are all made of Inconel 600. The shell plates are SB-168 UNS N06600, and the nozzle is SB-167 UNS N06600 seamless pipe. No volumetric examination was specified for the shell longitudinal seam, so a weld joint efficiency of 70% was applied to the required thickness calculations for the shell per UW-12. No volumetric examination was specified for the shell to head girth seams, so a weld joint efficiency of 85% was applied in the required thickness calculations for the heads per UW-12(d).

4. The nozzle flange and bolted cover are made of SA-182 F304 (304 stainless steel). The flange is a modified 12 inch OD blind Conflat flange, and the flat cover is a 12 inch OD blind Conflat flange. The suitability of the flange has been verified for the design conditions using Appendix 2 rules for hubless loose flanges, assuming the use of an elastomeric gasket in the bolted joint assembly. The flange-to-nozzle attachment welds were calculated to meet the weld sizing requirements of Appendix 2. The bolting materials selected for attaching the flat cover to the flange are SA-193 B8 (304 stainless steel) and have a major diameter of 5/16 in. The suitability of the Conflat Blind flange was verified by calculating it as a flat bolted head with an edge moment.

5. The NPS5 pipe nozzle opening is the shell is adequately reinforced, and the attachment welds have sufficient strength, as demonstrated by the attached calculations. The nozzle attachment weld design is consistent with Fig. UW-16.1, sketch (c), consisting of a full penetration weld in combination with an external fillet weld having a leg dimension calculated to meet the weld sizing requirements of UW-16. The openings in the flat head are exempted from opening reinforcement calculations per UG-36(c)(3)(a) due to their small size.

Design Summary Sheet

Molten Salt Loop Storage Tank
Designed per
ASME Section VIII, Division 1 (2010 Edition, 2011 Addenda)

6. Preheating and postweld heat treatment are neither required nor recommended for the vessel shell, heads and nozzle joints per UNF-56. Preheat and postweld heat treatment of the flange to nozzle welds is also not required nor recommended per UHA-32.

7. All welds shall be deposited by welders whose performance has been qualified in accordance with the requirements of ASME Section IX. The welding procedure specifications shall also be qualified per the requirements of ASME Section IX, and shall demonstrate a room temperature ultimate tensile strength of not less than 20,000 psi. The flange to nozzle weld shall be deposited following a welding procedure specification qualified for welding between these dissimilar metals.

8. A hydrostatic pressure test shall be applied to the completed vessel assembly as discussed in the hydrostatic pressure test information sheet. Test temperature should be at least 50°F but shall not be greater than 120°F.

9. Calculations have been provided to assist the user in selecting a pressure relieving device with an appropriate set pressure during installation.

August 24, 2012: I hereby certify the design information provided in this report to be complete, true, and accurate as represented, and compliant with the specified Code requirements.

John P. Swezy, Jr.
Mechanical Engineer
Fabrication Hoisting and Rigging Division
UT-Battelle, LLC

Section VIII, Division 1 (2010 Edition, 2011 Addenda)
Shell Thickness Calculations per UG-27 (and Appendix 1)

$t := 0.230$ Minimum Required Thickness of Cylindrical Shell, in.

$P := 35$ Max Internal Design Pressure, psi

$R := 9.75$ Inside Radius of Shell, in. (0.25 in. Nominal thickness)

$R_o := 10$ Outside Radius of Shell, in. (20 in. Nominal OD)

$S := 2160$ Max Allow. Stress, psi, SB-168 UNS N06600 @ 1160°F Sect.II-D, Table 1B)

$E := 0.70$ Joint Efficiency (Type 1 weld, No RT)

Circumferential Stress (Longitudinal Joints) [UG-27(c)(1)]
When the thickness is ≤ 0.5R, or P is ≤ 0.385SE the following formulas apply:

Checking: $0.5 \cdot R = 4.875$ $0.385 \cdot S \cdot E = 582.12$

Thickness Pressure Rating

$\frac{P \cdot R}{S \cdot E - 0.6P} = 0.229$ or $\frac{S \cdot E \cdot t}{R + 0.6t} = 35.17$

Longitudinal Stress (Circumferential Joints) [UG-27(c)(2)]
When the thickness is ≤ 0.5R, or P is ≤ 1.2SE, the following formulas apply:

Checking: $0.5 \cdot R = 4.875$ $1.2 \cdot S \cdot E = 1.814 \times 10^3$

Thickness Pressure Rating

$\frac{P \cdot R}{2S \cdot E + 0.4P} = 0.112$ or $\frac{2S \cdot E \cdot t}{R - 0.4t} = 72.015$

Cylindrical Shells calculated using Outside Radius (Appendix 1-1, Section VIII, Division 1);
Circumferential Stress (Longitudinal Joints)
When t is ≤ 0.5R, or P is ≤ 0.385SE, the following formulas apply:

Checking: $0.5 \cdot R = 4.875$ $0.385 \cdot S \cdot E = 582.12$

Thickness Pressure Rating

$\frac{P \cdot R_o}{S \cdot E + 0.4P} = 0.229$ or $\frac{S \cdot E \cdot t}{R_o - 0.4t} = 35.099$

Specified nominal shell thickness is 0.25 in., and therefore acceptable.

Section VIII, Division 1 (2010 Edition, 2011 Addenda)
Shell Thickness Calculations per UG-27 (and Appendix 1)(seamless for reinforcement)

$t := 0.161$ Minimum Required Thickness of Cylindrical Shell, in.

$P := 35$ Max Internal Design Pressure, psi

$R := 9.75$ Inside Radius of Shell, in. (0.25 in. Nominal thickness)

$R_o := 10$ Outside Radius of Shell, in. (20 in. Nominal OD)

$S := 2160$ Max Allow. Stress, psi, SB-168 UNS N06600 @ 1160°F Sect.II-D, Table 1B)

$E := 1.0$ Joint Efficiency (seamless per UG-37)

Circumferential Stress (Longitudinal Joints) [UG-27(c)(1)]
When the thickness is ≤ 0.5R, or P is ≤ 0.385SE the following formulas apply:

Checking: $0.5 \cdot R = 4.875$ $0.385 \cdot S \cdot E = 831.6$

Thickness Pressure Rating

$\frac{P \cdot R}{S \cdot E - 0.6P} = 0.16$ or $\frac{S \cdot E \cdot t}{R + 0.6t} = 35.318$

Longitudinal Stress (Circumferential Joints) [UG-27(c)(2)]
When the thickness is ≤ 0.5R, or P is ≤ 1.2SE, the following formulas apply:

Checking: $0.5 \cdot R = 4.875$ $1.2 \cdot S \cdot E = 2.592 \times 10^3$

Thickness Pressure Rating

$\frac{P \cdot R}{2S \cdot E + 0.4P} = 0.079$ or $\frac{2S \cdot E \cdot t}{R - 0.4t} = 71.81$

Cylindrical Shells calculated using Outside Radius (Appendix 1-1, Section VIII, Division 1);
Circumferential Stress (Longitudinal Joints)
When t is ≤ 0.5R, or P is ≤ 0.385SE, the following formulas apply:

Checking: $0.5 \cdot R = 4.875$ $0.385 \cdot S \cdot E = 831.6$

Thickness Pressure Rating

$\frac{P \cdot R_o}{S \cdot E + 0.4P} = 0.161$ or $\frac{S \cdot E \cdot t}{R_o - 0.4t} = 35.001$

Specified nominal shell thickness is 0.25 in., and therefore acceptable.

Section VIII, Division 1 (2010 Edition, 2011 Addenda)
2:1 Elliptical Head Thickness Calculations per UG-32

$t := 0.187$	Minimum Required Thickness after Forming, in.
$P := 35$	Internal Design Pressure (see UG-21), psi
$D := 19.5$	Inside Diameter of Head Skirt, in.
$S := 2160$	Max Allow. Stress, psi (SB-168 UNS N06600 @ 1160F Sect. II-D, Table 1B)
$E := 0.85$	Lowest Efficiency of any Joint in Head [per UW-12(d), Type 1, No RT]

2:1 Ellipsoidal Head, Concave to Pressure

Thickness or Pressure Rating

$$\frac{P \cdot D}{2 \cdot S \cdot E - 0.2 \cdot P} = 0.186 \qquad \frac{2 \cdot S \cdot E \cdot t}{D + 0.2 \cdot t} = 35.146$$

Selected nominal thickness for head is 0.25 in., reduced by 10% for thinout due to forming, results in a least nominal thickness of 0.225 in., and therefore acceptable.

TABLE UG-45
NOZZLE MINIMUM THICKNESS REQUIREMENTS

Nominal Size	Minimum Wall Thickness [see UG-16(d)] in.	mm
NPS 1/8 (DN 6)	0.060	1.51
NPS 1/4 (DN 8)	0.077	1.96
NPS 3/8 (DN 10)	0.080	2.02
NPS 1/2 (DN 15)	0.095	2.42
NPS 3/4 (DN 20)	0.099	2.51
NPS 1 (DN 25)	0.116	2.96
NPS 1 1/4 (DN 32)	0.123	3.12
NPS 1 1/2 (DN 40)	0.127	3.22
NPS 2 (DN 50)	0.135	3.42
NPS 2 1/2 (DN 65)	0.178	4.52
NPS 3 (DN 80)	0.189	4.80
NPS 3 1/2 (DN 90)	0.198	5.02
NPS 4 (DN 100)	0.207	5.27
NPS 5 (DN 125)	0.226	5.73
NPS 6 (DN 150)	0.245	6.22
NPS 8 (DN 200)	0.282	7.16
NPS 10 (DN 250)	0.319	8.11
≥ NPS 12 (DN 300)	0.328	8.34

GENERAL NOTE: For nozzles having a specified outside diameter not equal to the outside diameter of an equivalent standard NPS (DN) size, the NPS (DN) size chosen from the table shall be one having an equivalent outside diameter larger than the nozzle outside diameter.

Section VIII, Division 1 (2010 Edition, 2011 Addenda):
NPS5 Pipe Nozzle Thickness Calculations per UG-27 and UG-45

$t := 0.045$ Minimum Required Thickness of Nozzle, in.

$P := 35$ Max Internal Design Pressure, psi

$R := 2.56$ Inside Radius of Nozzle, in.(SCH 40 Nominal, reduced for undertolerance)

$R_o := 2.78$ Outside Radius of Nozzle, in. (NPS5 Nominal)

$S := 2160$ Max Allow. Stress, psi (SB-167 UNS N06600 @ 1160ºF per Sect II-D, Table 1B)

$E := 1.0$ Joint Efficiency [Seamless, see UW-12(d)]

$c := 0$ Specified corrosion allowance, in.

Circumferential Stress (Longitudinal Joints)
When the thickness is ≤ 0.5R, or P is ≤ 0.385SE the following formulas apply:

Checking: $0.5 \cdot R = 1.28$ $0.385 \cdot S \cdot E = 831.6$

Thickness or Pressure Rating

$\frac{P \cdot R}{S \cdot E - 0.6P} = 0.042$ $\frac{S \cdot E \cdot t}{R + 0.6t} = 37.572$

Longitudinal Stress (Circumferential Joints)
When the thickness is ≤ 0.5R, or P is ≤ 1.2SE, the following formulas apply:

Checking: $0.5 \cdot R = 1.28$ $1.2 \cdot S \cdot E = 2.592 \times 10^3$

Thickness or Pressure Rating

$\frac{P \cdot R}{2S \cdot E + 0.4P} = 0.021$ $\frac{2S \cdot E \cdot t}{R - 0.4t} = 76.475$

Cylindrical Shells calculated using Outside Radius (Appendix 1-1, Section VIII, Division 1);
Circumferential Stress (Longitudinal Joints)
When t is ≤ 0.5R, or P is ≤ 0.385SE, the following formulas apply:

Checking: $0.5 \cdot R = 1.28$ $0.385 \cdot S \cdot E = 831.6$

Thickness or Pressure Rating

$\frac{P \cdot R_o}{S \cdot E + 0.4P} = 0.045$ $\frac{S \cdot E \cdot t}{R_o - 0.4t} = 35.192$

UG-45 Nozzle Neck Thickness Requirements:

The minimum wall thickness for nozzle necks, t_{UG45}, shall be:

For access openings and openings used only for inspection:

$t_{UG45} = t_a$

Where:

t_a = minimum neck thickness required for internal and external pressure using UG-27 and UG-28 (plus corrosion allowance), as applicable. The effects of external forces and moments from supplemental loads (see UG-22) shall be considered. Shear stresses caused by UG-22 loadings shall not exceed 70% of the allowable tensile stress for the nozzle material.

$t_a = 0.045$

For other Nozzles:

$t_{UG45} = max\ (t_a, t_b)$

Where:

$t_b = min\ [t_{b3}, max\ (t_{b1}, t_{b2})]$ so, $t_b = 0.161$

t_{b1} = for vessels under internal pressure, the thickness (plus corrosion allowance) required for pressure (assuming $E = 1.0$) for the shell or head at the locations where the nozzle neck or other connection attaches to the vessel, but in no case less than the minimum thickness specified in UG-16(b).

$t_{b1} = 0.161$

t_{b2} = for vessels under external pressure, the thickness (plus corrosion allowance) obtained by using the external design pressure as an equivalent internal design pressure (assuming $E = 1.0$) in the formula for the shell or head at the location where the nozzle neck or other connection attaches to the vessel, but in no case less than the minimum thickness specified in UG-16(b).

$t_{b2} = 0$

t_{b3} = the thickness given in Table UG-45 plus the thickness added for corrosion allowance.

$t_{b3} = 0.226$

So, $t_{UG45} = 0.161$

The nominal wall thickness of NPS5, SCH 40, SB-167 seamless pipe is 0.258", reduced to 0.223" for undertolerance, and therefore acceptable.

Nozzle Attachment Weld Detail

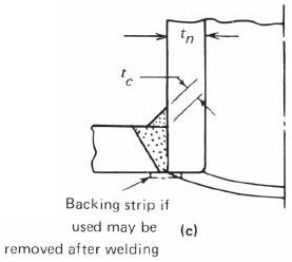

Nozzle attachment welds shall be consistent with Fig. UW-16.1, sketch (c)

Fillet throat shall be not < t_c, where "t_c" is not < the smaller of 0.25 in. or 0.7 t_{min}, and "t_{min}" is the lesser of the thicknesses to be joined by welding or 0.75"

NPS5 Pipe Nozzle External Fillet Weld Sizing Calculations:
Nominal Shell Thickness = 0.25"; Nominal NPS5 SCH 40 pipe thickness = 0.258"
Shell thickness is less, so t_{min} = 0.25"; 0.7 t_{min}= 0.175", which is < 0.25" so t_c= 0.175".
Fillet throat = 0.707(leg), so fillet leg = throat/0.707 = 0.175/0.707 = 0.247".

The external fillet weld shall have equilateral leg dimensions of not less than 0.25 (1/4) in.

Section VIII, Division 1 (2010 Edition, 2011 Addenda)
Opening Reinforcement Calculations per UG-37

$D := 19.5$	Inside Shell Diameter, in.
$D_p := 0$	Outside Diameter of Reinforcing Pad, in.
$d := 5.047$	Diameter of Finished Opening, in. (adjusted for undertolerance)
$E_1 := 1.0$	Efficiency of Weld Joint if Penetrated by Nozzle
$F := 1.0$	Correction Factor for Nozzle Orientation
$h := 0$	Inward Nozzle Protrusion from Inner Shell Surface, in.
$P := 35$	Internal Design Pressure, psi
$R := 9.75$	Inside Radius of Shell Course, in.
$R_n := 2.52$	Inside Radius of Nozzle under Consideration, in.
$S_n := 2160$	Max Stress (Nozzle), psi (SB-167 @ 1160ºF per Sec.II, Part D, Table1B)
$S_v := 2160$	Max Stress (Vessel), psi (SB-168 @ 1160ºF per Sec.II, Part D, Table1B)
$S_p := 0$	Max Stress (Repad), psi
$f_{r1} := \frac{S_n}{S_v} = 1$	Strength Reduction Factor for Nozzle (1.0 for Abutted/Partial Insert Nozzle)
$f_{r2} := \frac{S_n}{S_v} = 1$	Strength Reduction Factor for Nozzle Attachment Welds
$f_{r3} := \frac{S_p}{S_v} = 0$	Strength Reduction Factor for Repads [(lesser of S_n or S_p)/S_v]
$f_{r4} := \frac{S_p}{S_v} = 0$	Strength Reduction Factor for Repad Attachment Welds
$t := 0.25$	Specified Vessel Shell Thickness, in.
$t_e := 0$	Thickness or Height of Reinforcing Pad, in.
$t_i := 0$	Nominal Thickness of Inward Nozzle Projection, in.
$t_r := 0.161$	Required Thickness of Seamless Shell (see UG-27), in.
$t_n := 0.258$	Nominal Thickness of Nozzle Wall, in.
$t_{rn} := 0.045$	Required Thickness of Seamless Nozzle Wall (see UG-27 & UG-45), in.

Total Required Reinforcement for Openings under Internal Pressure (A) [see UG-37(c)]

$A := d \cdot t_r \cdot F + 2 \cdot t_n \cdot t_r \cdot F \cdot (1 - f_{r1})$ so $A = 0.813$

Limitations of Reinforcement Parallel to the Shell (X)(see Figure UG-37.1):

Use the ***larger*** quantity of the following:

$d = 5.047$ or $R_n + t_n + t = 3.028$ so $X := 5.047$

Limitations of Reinforcement Perpendicular to the Shell (Y)(see Figure UG-37.1):

Outward projection from the shell (Y_1), use the ***smaller*** of the following:

$2.5 \cdot t = 0.625$ or $2.5 \cdot t_n + t_e = 0.645$ so $Y_1 := 0.625$

Inward projection from the inner surface of the shell (Y_2), use the ***smaller*** of the following:

$h = 0$ or $2.5t = 0.625$ or $2.5t_i = 0$ so $Y_2 := 0$

$Y := Y_1 + Y_2$ so $Y = 0.625$

Area Available in the Shell Due to Excess Thickness (A_1)(see Fig. UG-37.1):

Use the ***larger*** quantity from the following Formulas

$d \cdot (E_1 \cdot t - F \cdot t_r) - 2 \cdot t_n \cdot (E_1 \cdot t - F \cdot t_r) \cdot (1 - f_{r1}) = 0.449$

$2 \cdot (t + t_n) \cdot (E_1 \cdot t - F \cdot t_r) - 2 \cdot t_n \cdot (E_1 \cdot t - F \cdot t_r) \cdot (1 - f_{r1}) = 0.09$ so $A_1 := 0.449$

Area Available in the Nozzle due to Excess Thickness (A_2)(see Fig. UG-37.1):

Use the ***smaller*** quantity from the following Formulas

$5 \cdot (t_n - t_{rn}) \cdot f_{r2} \cdot t = 0.266$

$5 \cdot (t_n - t_{rn}) f_{r2} \cdot t_n = 0.275$

$2 \cdot (t_n - t_{rn}) \cdot (2.5 \cdot t_n + t_e) \cdot f_{r2} = 0.275$ so $A_2 := 0.266$

Area Available from Inward Nozzle Projection (A_3)(see Fig. UG-37.1):

Use the ***smaller*** quantity from the following Formulas

$5 \cdot t \cdot t_i \cdot f_{r2} = 0$

$5 \cdot t_i \cdot t_i \cdot f_{r2} = 0$

$2 \cdot h \cdot t_i \cdot f_{r2} = 0$ so $A_3 := 0$

Area Available from Added Reinforcement Pads (A_5)(see Fig. UG-37.1)

(N/A for Nozzle attachments without added reinforcement pads)

$A_5 := (D_p - d - 2 \cdot t_n) \cdot t_e \cdot f_{r4}$ so $A_5 = 0$

Area Available from Outer Nozzle Attachment Welds (A_{41})(see Fig. UG-37.1)

where $l_1 := 0.3125$ Leg Length for Outer Nozzle Attachment Fillet Weld

$l_1^2 \cdot f_{r2} = 0.098$ when a reinforcing pad ***is not*** attached

$l_1^2 \cdot f_{r3} = 0$ when a reinforcing pad ***is*** attached so $A_{41} := 0.098$

Area Available from Reinforcing Pad Attachment Fillet Welds (A_{42})(see Fig. UG-37.1)

(N/A for Nozzle attachments without added reinforcement pads)

where $l_3 := 0$ Leg Length for Reinforcing Pad Attachment Weld

$A_{42} := l_3^2 \cdot f_{r4}$ so $A_{42} = 0$

Area Available from Inner Nozzle Attachment Welds (A_{43})(see Fig. UG-37.1)

(Applicable for through nozzle attachment. N/A for abutting or partial insertion methods)

where $l_2 := 0$ Leg Length for inner Nozzle Attachment Fillet Weld

$A_{43} := l_2^2 \cdot f_{r2}$ so $A_{43} = 0$

Total Reinforcement Available (A_t)

$A_t := A_1 + A_2 + A_3 + A_5 + A_{41} + A_{42} + A_{43} = 0.813$ and $A = 0.813$

Since $A_t \geq A$, Opening is Adequately Reinforced

Weld Strength Requirements

For Through Nozzle Attachments, [see UG-41(b)(1) and (2)]

$W_t := \left[A - A_1 + 2 \cdot t_n \cdot f_{r1} \cdot \left(E_1 \cdot t - F \cdot t_r\right)\right] \cdot S_v$ so $W_t = 884.501$

Weld Path 1-1 Strength (W_{1t})

$W_{1t} := \left(A_2 + A_5 + A_{41} + A_{42}\right) S_v$ so $W_{1t} = 786.24$

Weld Path 2-2 Strength (W_{2t})

$W_{2t} := \left(A_2 + A_3 + A_{41} + A_{43} + 2 \cdot t_n \cdot t \cdot f_{r1}\right) S_v$ so $W_{2t} = 1.065 \times 10^3$

Weld Patth 3-3 Strength (W_{3t})

$W_{3t} := \left(A_2 + A_3 + A_5 + A_{41} + A_{42} + A_{43} + 2 \cdot t_n \cdot t \cdot f_{r1}\right) S_v$ so $W_{3t} = 1.065 \times 10^3$

Strength Available

$d_{nm} := d + t_n$ $d_{nm} = 5.305$ Mean Nozzle Diameter, in.

$D_n := d + 2t_n$ $D_n = 5.563$ Nozzle OD, in.

$L_g := 0.25$ Weld leg of nozzle to shell groove weld, in.

Nozzle in Shear

$W_{ns} := \frac{\pi}{2} \cdot d_{nm} \cdot t_n \cdot S_v \cdot 0.70$ $W_{ns} = 3.251 \times 10^3$

Nozzle to shell groove weld in tension (assuming through nozzle)

$W_{gtt} := \frac{\pi}{2} \cdot D_n \cdot L_g \cdot S_v \cdot 0.74$ $W_{gtt} = 3.492 \times 10^3$

Nozzle to shell groove weld in tension (assuming abutting nozzle)

$W_{gta} := \frac{\pi}{2} \cdot d_{nm} \cdot t_n \cdot S_v \cdot 0.74$ $W_{gta} = 3.436 \times 10^3$

Nozzle to shell fillet weld in shear

$W_{nr} := \frac{\pi}{2} \cdot D_n \cdot l_1 \cdot S_v \cdot 0.49$ $W_{nr} = 2.89 \times 10^3$

Repad to shell fillet weld in shear

$W_{rf} := \frac{\pi}{2} \cdot D_p \cdot l_3 \cdot S_v \cdot 0.49$ $W_{rf} = 0$

Actual Strength of Connecting Elements

Through Nozzles

Strength of Path 1-1

$W_{1s} := W_{ns} + W_{rf}$ $W_{1s} = 3.251 \times 10^3$

W_{1s} shall be > the lesser of W_t or W_{1t}

$W_t = 884.501$ $W_{1t} = 786.24$

Strength of Path 2-2

$W_{2tt} := W_{gtt} + W_{nr}$ $W_{2tt} = 6.382 \times 10^3$

W_{2tt} shall be > the lesser of W_t or W_{2t}

$W_t = 884.501$ $W_{2t} = 1.065 \times 10^3$

Strength of Path 3-3

$W_{3tt} := W_{gtt} + W_{rf}$ $W_{3tt} = 3.492 \times 10^3$

W_{3tt} shall be > the lesser of W_t or W_{3t}

$W_t = 884.501$ $W_{3t} = 1.065 \times 10^3$

Therefore, the weld strength is adequate

Section VIII, Division 1 Unfired Pressure Vessels (2010 Edition, 2011 Addenda):
Shell Vacuum Calculations per UG-28

$D_o := 20$ Outside Diameter of Cylindrical Shell Course, in.

$L := 28$ Total (or Design) Length of Shell Course, in. (including Head Straight Flange)

$P := 15$ External Design Pressure, psi.

$S := 2160$ Max Allowable Stress Value at Design Temperature, psi

$t := 0.161$ Minimum Required thickness of Cylindrical Shell or Tube, in.

$t_n := 0.25$ Nominal Thickness of Cylindrical Shell or Tube, in.

Cylindrical Shell or Tube thickness [UG-28(c)]

Determine the Ratios D_o/t and L/D_o:

Assume a value for "t" $t = 0.161$

Calculate $\frac{D_o}{t} = 124.224$ and $\frac{L}{D_o} = 1.4$

If $D_o/t > 10$, proceed as follows. (If D_o/t is < 10, see below)

Determine the Value of "A" from Figure G, Section II, Part D:

$A := 0.0007$

Determining the Value of "B" from External Pressure Chart NFN-4 in Section II, Part D:

$B := 5000$ (selected conservative value for design temperature)

Calculate the Value of "P_a" the Allowable External Working Pressure, psi

$$P_a := \frac{4 \cdot B}{3 \cdot \left(\frac{D_o}{t} \right)} = 53.667$$

Since $P_a \geq P$, the assumed value for "t" is acceptable for vacuum service.

Section VIII, Division 1 (2010 Edition, 2011 Addenda)
Elliptical Head Vacuum Calculations per UG-33

$t := 0.113$ Minimum Required Thickness after Forming, in.

$P := 25$ Internal Design Pressure, psi [1.67 x External Pressure per UG-33(a)(1)(a)]

$D := 19.5$ Inside Diameter of Head Skirt, in.

$D_o := 20$ Outside Diameter of Head Skirt, in.

$S := 2160$ Max Allow Stress, psi (SB-168 UNS N06600 @ 1160ºF Sect. II-D, Table 1B)

$E := 1.0$ Lowest Efficiency of any Joint in Head [per UG-33(a)(1)(a)]

$h := 5.0$ Inside Depth of Head Knuckle from Tangent, in. (2:1 Ell. w/o SF)

$h_o := 5.25$ Outside Height of Head from Tangent, in. (2:1 Ell. w/o SF)

$\frac{D_o}{2 \cdot h_o} = 1.905$ and $K_o := 0.86$ Factor (based upon Do/2ho, from Table UG-33.1)

$R_o := K_o \cdot D_o = 17.2$

Required head thickness for external pressure shall be the greater of:

2:1 Ellipsoidal Head, Concave to Pressure [UG-33(a)(1)(a)]

Thickness Pressure Rating

$\frac{P \cdot D}{2 \cdot S \cdot E - 0.2 \cdot P} = 0.113$ or $\frac{2 \cdot S \cdot E \cdot t}{D + 0.2 \cdot t} = 25.005$

External Pressure Calculations (convex to head) (assumed thickness of 0.8")[UG-33(d)]

$A := \frac{0.125}{\frac{R_o}{t}} = 8.212 \times 10^{-4}$

Per External Pressure Chart NFN-4 in Sect. II, Part D:

$B := 5000$ (selected conservative value for design temperature)

Calculate the Value of Allowable External Working Pressure "P_a", psi

$P_a := \left[\frac{4 \cdot B}{3 \cdot \left(\frac{D_o}{t} \right)} \right] = 37.667$

P_a accepable for assumed head thickness = 0.113 in., and the selected head thickness is 0.25" reduced by 10% for thinout due to forming to 0.225 in. , and therefore acceptable for vacuum service.

Section VIII, Division 1 Unfired Pressure Vessels (2010 Edition, 2011 Addenda):
NPS5 Nozzle Vacuum Calculations per UG-28

$D_o := 5.563$ Outside Diameter of Nozzle, in.

$L := 7$ Total (or Design) Length of Nozzle, in.

$P := 15$ External Design Pressure, psi.

$S := 2160$ Max Allowable Stress Value at Design Temperature, psi

$t := 0.045$ Minimum Required thickness of Nozzle, in.

$t_n := 0.258$ Nominal Thickness of Nozzle, in.

Cylindrical Shell or Tube thickness [UG-28(c)]

Determine the Ratios D_o/t and L/D_o:

Assume a value for "t" $t = 0.045$

Calculate $\frac{D_o}{t} = 123.622$ and $\frac{L}{D_o} = 1.258$

If $D_o/t > 10$, proceed as follows. (If D_o/t is < 10, see below)

Determine the Value of "A" from Figure G, Section II, Part D:

$A := 0.00075$

Determining the Value of "B" from External Pressure Chart NFN-4 in Section II, Part D:

$B := 5000$ (selected conservative value for design temperature)

Calculate the Value of "P_a" the Allowable External Working Pressure, psi

$$P_a := \frac{4 \cdot B}{3 \cdot \left(\frac{D_o}{t} \right)} = 53.928$$

Since $P_a \geq P$, the assumed value for "t" is acceptable for vacuum service.

Conflat Blind Flange Dimensions

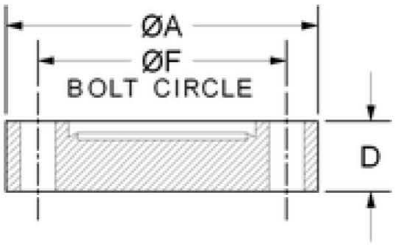

12" OD Conflat Flange
Non – Rotatable
32 Clearance Holes (0.332 Diameter)
BLANK

- A: 11.97"
- **D: 1.02"**
- F: 11.181"

\

Flange Attachment Weld Details

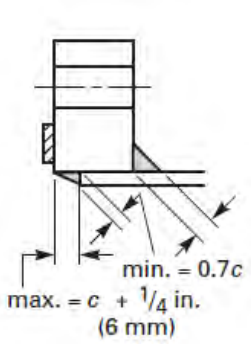

Fillet weld sizing Calculations:

Minimum nozzle inset from flange face to nozzle end shall be t_n for the applicable nozzle

Maximum nozzle inset from flange face to nozzle end shall be t_n + 1/4"

Minimum fillet weld leg at ID of flange shall be a full fillet weld (not < t_n)

Minimum fillet weld leg at OD of Flange at the hub on the back side of the flange shall be 0.7c, where "c" is the lesser of t_n or t_x (t_x = 2 t_n for hubless loose flanges)

Pipe Size	*Min. Inset (t_n)*	*Max. Inset (t_n+1/4")*	*ID Fillet Leg (t_n)*	*Back Side Fillet Leg (0.7t_n)*
NPS5 SCH 40	0.258"	0.508" (use 1/2")	0.258" (use 1/4")	0.181" (use 3/16")

A fillet weld leg dimension of 1/4 in. has been chosen for the back side fillet weld.

Section VIII, Division 1 (2010 Edition, 2011 Addenda)
Flange Design Calculations per Appendix 2 (Hubless, Loose)

$A := 11.97$ OD of Flange, in.

$A_b := 1.88$ Cross Sectional Area of Bolt at Smallest Diameter, in^2 (3/8 inch MAJ DIA)

$B := 5.563$ Inside Diameter of Flange, in. (if < $20g_1$, substitute B_1 for B in formula for S_H)

$B_1 := 5.821$ Sum of B + g_1 (or g_o, depending on value of "f" and Flange Type)

$b := 0.5$ Effective Gasket or Contact Seating Width, in.

$b_o := 0.5$ Basic Gasket Seating Width, in.

$C := 11.181$ Bolt Circle Diameter, in.

$G := 10.75$ Diameter at location of Gasket Load Reaction, in.

$g_o := 0.258$ Thickness of Hub at Small End, in. (Nozzle Thickness)

$g_1 := 0.508$ Thickness of Hub at Back of Flange, in. (Nozzle Thickness plus Fillet Weld Leg)

$h := 0.25$ Hub Length, in. (fillet Weld Leg)

$h_G := \frac{C - G}{2}$ so $h_G = 0.215$ Radial Distance from Gasket Load Reaction to Bolt Circle, in.

$h_o := \sqrt{B \cdot g_o}$ so $h_o = 1.198$ Factor, in.

Use the following for determining "F_L" and "V_L" $\frac{h}{h_o} = 0.209$ $\frac{g_1}{g_o} = 1.969$

:

$E := 21400000$ Modulus of Elasticity for Flange Material, psi (SA-182 F304 @ 1160ºF)

$F_L := 3.7$ Factor for Loose Type Flanges (from Figure 2-7.4)

$K := \frac{A}{B}$ so $K = 2.152$ Ratio of Flange OD to ID

$K_L := 0.2$ Flange Rigidity Factor, Loose Flanges [see 2-14(b)]

$m := 0$ Gasket Factor, from Table 2-5.1

$N := 0.5$ Width, in., from Table 2-5.1, (potential contact width)

$P := 35$ Internal Design Pressure, psi

$R := \frac{C - B}{2} - g_1$ so $R = 2.301$ Radial Distance, Bolt Circle to Hub OD @ back of Flange, in.

$S_a := 20000$ Max Allow. Bolt Stress, psi (SA-193 B8 @ 70ºF per Sect. II-D, Table 3)

$S_b := 7360$ Max Allow. Bolt Stress, psi (SA-193 B8 @ 1160ºF per Sect.II-D, Table 3)

$S_f := 7380$ Max Allow. Flange Stress, psi (SA-182 F304 @ 1160ºF per Sect.II-D, Table 1A)

$S_n := 2160$ Max Allow. Nozzle Stress, psi (SB-167 UNS N06600 @ 1160ºF, Sect.II-D, Table 1B)

$T := \frac{K^2 \cdot (1 + 8.55246 \cdot \log(K)) - 1}{(1.04720 + 1.9448 \cdot K^2) \cdot (K - 1)}$ (From Figure 2-7.1) so $T = 1.452$

$t := 1.02$ Thickness of Flange, in.

$t_n := 0.258$ Nominal Thickness of Nozzle to which Flange is attached, in.

$$U := \frac{K^2 \cdot (1 + 8.55246 \cdot \log(K)) - 1}{1.36136 \cdot \left(K^2 - 1\right) \cdot (K - 1)} = 2.953$$ (From Figure 2-7.1)

$V_L := 12$ Factor for ***Loose*** Type Flanges (from Figure 2-7.5)

$w := 0.5$ Width, in., (basic gasket seating width)

$$Y := \frac{1}{K - 1} \cdot \left(0.66845 + 5.71690 \cdot \frac{K^2 \cdot \log(K)}{K^2 - 1} \right) = 2.687$$ (From Figure 2-7.1)

$y := 0$ Gasket or Joint-Contact-Surface Unit Seating Load, psi (from Table 2-5.1)

$$Z := \frac{K^2 + 1}{K^2 - 1} = 1.551$$ (From Figure 2-7.1)

Total Bolt Load for Operating Conditions, (W_{m1}) [2-5(c)(1), Formula (1)]:

$$W_{m1} := 0.785 \cdot G^2 \cdot P + (2 \cdot b \cdot 3.14 \cdot G \cdot m \cdot P) = 3.175 \times 10^3$$

Total Bolt Load for Gasket Seating Conditions, (W_{m2}) [2-5(c)(2), Formula (2)]:

$$W_{m2} := 3.14 \cdot b \cdot G \cdot y = 0$$

Required Bolt Cross Section Area; Operating Conditions, sq.in. (A_{m1}) (2-3)

$$A_{m1} := \frac{W_{m1}}{S_b} = 0.431$$

Required Bolt Cross Section Area; Gasket Seating Conditions, sq.in. (A_{m2}) (2-3)

$$A_{m2} := \frac{W_{m2}}{S_a} = 0$$

Total Required Bolt Cross Section Area, sq.in. (A_m) (2-3)

the greater of $A_{m1} = 0.431$ or $A_{m2} = 0$ so $A_m := 0.431$

$n := 32$ **Number of Bolts** $A_b = 1.88$

Flange Design Bolt Load, lb. (W) [2-5(e)]

for ***operating conditions*** or for ***gasket seating conditions***

$W = W_{m1}$ & $W_{m1} = 3.175 \times 10^3$ $\frac{(A_m + A_b) \cdot S_b}{2} = 8.504 \times 10^3$

$W := 8.504 \times 10^3$ **Bolt Load Capability** $A_b \cdot S_b = 1.384 \times 10^4$

Factor "d" (2-3) for ***Loose*** Type Flanges

$$d := \frac{U}{V_L} \cdot h_o \cdot g_o^{\,2} = 0.02$$

Factor "e" (2-3) for ***Loose*** Type Flanges

$$e := \frac{F_L}{h_o} = 3.088$$

Total Hydrostatic End Force, lb. (H) (2-3)

$$H := 0.785 \cdot G^2 \cdot P = 3.175 \times 10^3$$

Hydrostatic End Force on Area Inside of Flange, lb. (H_D) (2-3)

$$H_D := 0.785 \cdot B^2 \cdot P = 850.268$$

Gasket Load, lb. (H_G) (2-3)

$$H_G := W - H = 5.329 \times 10^3$$

Total Joint-Contact Surface Compression Load, lb. (H_P) (2-3)

$$H_P := 2 \cdot b \cdot 3.14 \cdot G \cdot m \cdot P = 0$$

Differential between Total Hydrostatic End Loads and End Loads inside Flange (H_T) (2-3)

$$H_T := H - H_D = 2.325 \times 10^3$$

Radial Distance from Bolt Circle to Flange ID, in. (h_D) for ***Loose*** Type Flanges

$$h_D := \frac{C - B}{2} = 2.809$$

Radial Distance from Bolt Circle to Circle upon which H_T acts, in. (h_T) for ***Loose*** Type Flanges

$$h_T := \frac{h_D + h_G}{2} = 1.512$$

Factor "L" (2-3)

$$L := \frac{t \cdot e + 1}{T} + \frac{t^3}{d} = 56.933$$

Component of Moment due to H_D, in.-lb. (M_D) (2-3)

$$M_D := H_D \cdot h_D = 2.388 \times 10^3$$

Component of Moment due to H_G, in.-lb. (M_G) (2-3)

$$M_G := H_G \cdot h_G = 1.148 \times 10^3$$

Component of Moment due to H_T, in.-lb. (M_T) (2-3)

$$M_T := H_T \cdot h_T = 3.516 \times 10^3$$

Total Flange Moment, in.-lb. (M_O) (2-6)

for ***Operating*** conditions for ***Gasket Seating*** conditions

$$M_G + M_T + M_D = 7.052 \times 10^3 \qquad W \cdot \frac{(C - G)}{2} = 1.833 \times 10^3 \qquad \text{so} \qquad M_o := 7.052 \times 10^3$$

Longitudinal Hub Stress, psi (S_H) (2-13) for ***Loose*** Type Flanges $S_H = 0$

Radial Flange Stress, psi (S_R) (2-13) for ***Loose*** Type Flanges $S_R = 0$

Tangential Flange Stress, psi (S_T) (2-13) for ***Loose*** Type Flanges

$$S_T := \frac{Y \cdot M_o}{t^2 \cdot B} = 3.274 \times 10^3$$

Stress Limitations (2-8) $S_f = 7.38 \times 10^3$

S_H shall be **≤ S_f** for ***cast iron***, and **≤ 1.5(S_f)** for ***other materials***. $1.5 \cdot S_f = 1.107 \times 10^4$

S_R and **S_T** shall be **≤** $S_f = 7.38 \times 10^3$

Flange Rigidity Index (J) (2-14):

$$J := \frac{109.4 \cdot M_o}{E \cdot t^3 \cdot \left(K_L \cdot \ln(K)\right)} = 0.222$$

(acceptable if Index if ≤ 1.0)

Selected flange thickness is 0.102, and the calculated flange stresses and rigidity index are acceptable.

Section VIII, Division 1, Unfired Pressure Vessels (2010 Edition, 2011 Addenda):
Flat Unstayed Head Calculations per UG-34

$C := 0.3$	Head Attachment Factor
$d := 10.75$	Diameter of Round Heads, or Short Span for Non-Circular Heads, in.
$E := 1.0$	Joint Efficiency for any Category A Weld Joint (see Table UW-12)
$h_g := 0.215$	Gasket Moment Arm, distance from bolt centerline to center of gasket seat, in.
$P := 35$	Max Allowable Working Pressure, psi (See PG-21)
$S := 7380$	Max Allowable Stress, psi (SA-182 F304 @ 1160ºF per Sect. II-D, Table 1A)
$t_h := 1.02$	Nominal Thickness of a Flat Head or Cover, in.
$t_r := 0.045$	Thickness Required for a Seamless Shell, in.
$t_s := 0.258$	Nominal Thickness of Shell, in.
$W := 8504$	Total Bolt Load, lb (See PG-31.3.2)

The Minimum Required Thickness for Flat Unstayed Circular Heads and Covers
(with a bolted edge moment)[UG-34(c)(2), Formula 2]:

$$d \cdot \sqrt{\frac{C \cdot P}{S \cdot E} + \frac{1.9 \cdot W \cdot h_g}{S \cdot E \cdot d^3}} = 0.456$$

Selected Flat Head thickness is 1.02 in., and therefore acceptable.

Hydrostatic Test Pressure Information:

1. Per paragraph UG-99 of Section VIII, Division 1 (2010 Edition, 2011 Addenda) the hydrostatic test pressure shall be 1.3 times MAWP times the lowest ratio of allowable stress at test temperature to allowable stress at design temperature for any component.

   SB-167 UNS N06600 S_a @ 70°F = 20,000 psi — Ratio: 20000/2160 = 9.26
   SB-167 UNS N06600 S_a @ 1160°F = 2,160 psi

   SB-168 UNS N06600 S_a @ 70°F = 20,000 psi — Ratio: 20000/2160 = 9.26
   SB-168 UNS N06600 S_a @ 1160°F = 2,160 psi

   SA-182 F304 S_a @ 70°F = 20,000 psi — Ratio: 20000/7380 = 2.71
   SA-182 F304 S_a @ 1160°F = 7,380 psi

   The controlling ratio for test pressure is 9.26, so the minimum Test Pressure shall be:
   TP = 35 x 1.3 x 9.26 = ***421.3 psig (use 422 psig)***

   Test pressure shall be adjusted as required to account for any hydrostatic head on the vessel at the connection point for the dial indicating pressure gage, to ensure that full test pressure is applied at the top of the vessel.

2. Per paragraph UG-99 (h) of Section VIII, Division 1 (2010 Edition, 2011 Addenda) the minimum metal temperature during the pressure test shall be not less than 30°F above the minimum design metal temperature (MDMT) for the limiting component. Per UHA-51(d) an MDMT of -20°F may be assigned to the flange and top cover. Per UNF-65, an MDMT of -20°F may be assigned to the shell, nozzle and heads. ***Pressure testing at normal ambient temperatures is acceptable. Maximum test temperature shall not exceed 120°F.***

3. Per paragraph UG-102(a) of Section VIII, Division 1 (2010 Edition, 2011 Addenda) a dial indicating test pressure gage shall have a maximum indicating range of about twice the test pressure; but shall be not less than 1-1/2 times the test pressure, and not greater than 4 times the test pressure. ***A dial indicating pressure gage with an indicating range of 0-1000 psi is recommended for use during the pressure tests.***

Section VIII, Division 1 Unfired Pressure Vessels (2010 Edition, 2011 Addenda): Overpressure Device Operation and Setpoint Calculations per UG-125 and UG-134

where

$P := 35$ MAWP marked on the Vessel, psi

Max permissible overpressure (P_{max1}) for single overpressure device installations, psi [see UG-125(c)]

P_{max1} shall be the ***greater*** of: $1.10 \cdot P = 38.500$ or $P + 3 = 38.000$ so $P_{max1} := 38.5$

Max permissible overpressure (P_{max2}) for multiple overpressure device installations, psi [see UG-125(c)(1)]

P_{max2} shall be the ***greater*** of: $1.16 \cdot P = 40.600$ or $P + 4 = 39.000$ so $P_{max2} := 40.6$

Max permissible overpressure (P_{max3}) for Fire Exposure, psi [see UG-125(c)(2)]

$P_{max3} := 1.21 \cdot P$ so $P_{max3} = 42.350$

Determining ***highest potential setpoint (P_1) for a single overpressure device installation***, psi [see UG-134(a)]

P_1 shall be $\leq P$ $P_1 := P$ so $P_1 = 35.000$

Determining ***highest potential setpoint (P_2) for multiple overpressure device installation***, psi [see UG-134(a)]

P_2 shall not be > 1.05(P) $P_2 := 1.05 \cdot P$ so $P_2 = 36.750$

Determining ***highest potential setpoint (P_3) for a fire exposure overpressure device***, psi [see UG-134(b)] (when ***all*** overpressure protection is provided by a ***single*** device, use P_1)

P_3 shall not be > 1.10(P) $P_3 := 1.10 \cdot P$ so $P_3 = 38.500$

Maximum permissible setpoint adjustment (T_s), psi [see UG-126(c)]

Marked setpoint of SV under consideration (P_s), psi $P_s := 35$

Max allowable adjustment is 5% $T_s := P_s \cdot 0.05$ so $T_s = 1.750$

Highest permissible setpoint (A_{hi}) $A_{hi} := P_s + T_s$ so $A_{hi} = 36.750$

Lowest permissible setpoint (A_{lo}) $A_{lo} := P_s - T_s$ so $A_{lo} = 33.250$

APPENDIX B. PUMP SUMP TANK PRESSURE CALCULATIONS

APPENDIX B. PUMP SUMP TANK PRESSURE CALCULATIONS

Pressure calculations were performed for the storage tank, sump tank, and piping system. The surge tank will operate at pressures below 15 psig, and specific calculations for this tank were not performed.

Summary

The sump tank will safely operate at 700°C for up to 5000 continuous h with up to 30 psig gas pressure inside the tank. The portions of the tank under stress leading to creep will self-relieve and no longer creep. A conservative approach is that the creep rate will be up to 3.0% for 5000 h of operation in only the highest stress areas. The remainder of the tank will have less than 0.3% creep for the same period of time. The effects of thermal cycling will be minimal because the heating and cooling are done slowly over the course of days. The tank may be safely operated more than 5000 continuous h, but it is recommended that it be inspected between runs to observe the effects of creep in the wall of the tank.

Calculations

Two stress analyses were performed, one at 30 psi and one at 45 psi. The 30 psi analysis will be discussed in detail, and the 45 psi model will demonstrate the worst case expected. The primary failure mode would be the creep-rupture case, which is not expected during the lifetime of the tank's operation.

The Molten Salt Loop Sump Tank was designed to operate for an extended period of time at 700°C, 30 psig with salt filling the lower portion of the tank and argon gas in the upper portion of the tank. For the purpose of the analysis, the bonding between the reinforcement struts and the tank wall is modeled as bonded.

Model

The model used for this calculation was a symmetric half slice of the overall tank and lid, as shown below in Fig. B.1. The small tab sticking out of the far side of the tank was not real geometry and was used to stabilize the model for the analysis.

The mesh used was very fine, and a mesh independence study was performed. The mesh used was found to be stable for two orders of magnitude less than what was used (Fig. B.2).

The failure criteria for the tank would be excessive creep leading to rupture. That would be based on the information shown in Fig. B.3. Stresses of 7 and 10 ksi have been marked in the figure by red circles. They are related to creep rates of 0.006% and 0.6%/1000 h operation at temperature, respectively. These points on this plot will be discussed in the results.

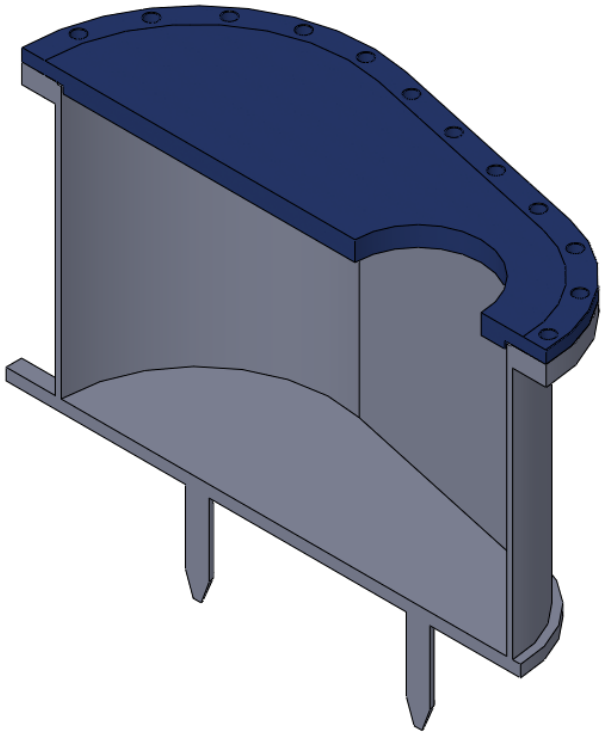

Fig. B.1. Cross section of the sump tank used for analysis, with lid.

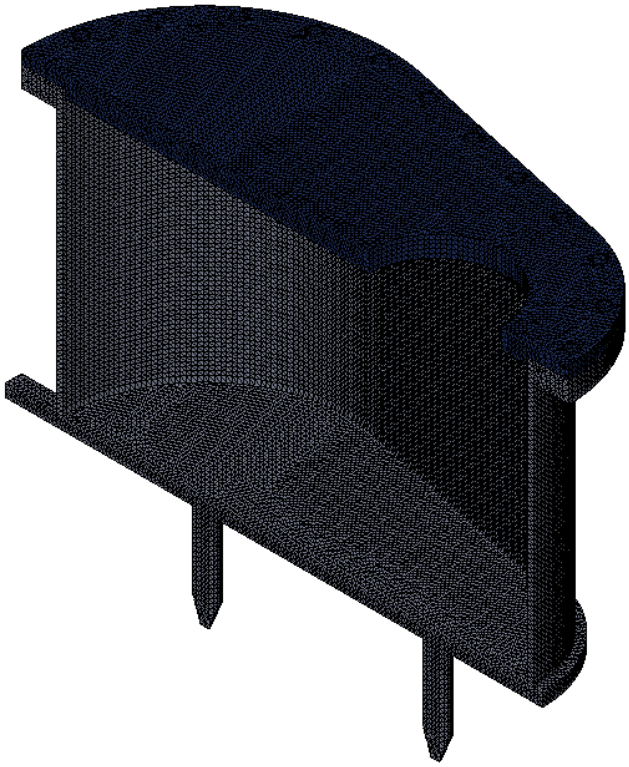

Fig. B.2. Fine mesh of the sump tank and lid.

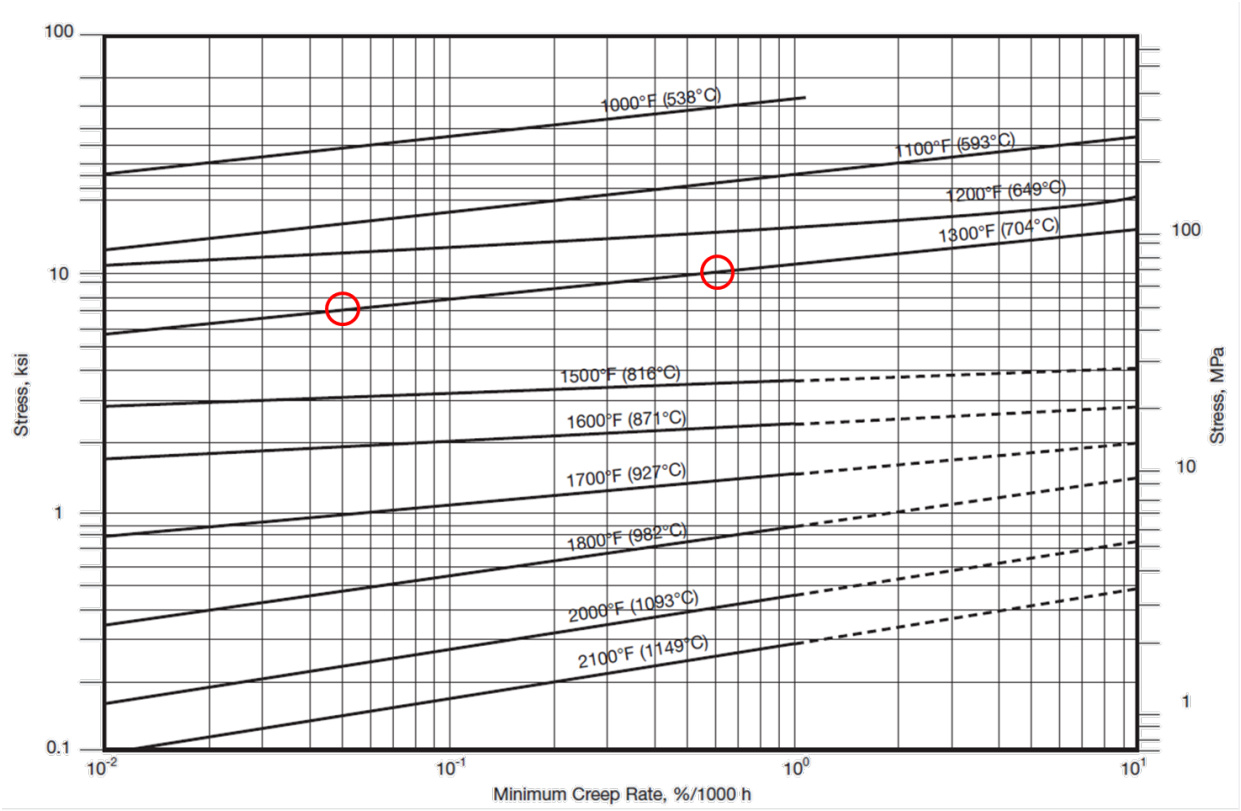

Fig. B.3. Plot of creep rates of Inconel 600 at various temperatures. The creep rates for 7 and 10 ksi are noted in red circles.

30 psi Results

The following are the results for the sump tank at 30 psi internal pressure.

General Results

The stress results of the tank are in Fig. B.4. Areas in red are above 12 ksi stress and will likely self-relieve during the initial hours of operation. The remaining areas are subject to creep based on the information in this section.

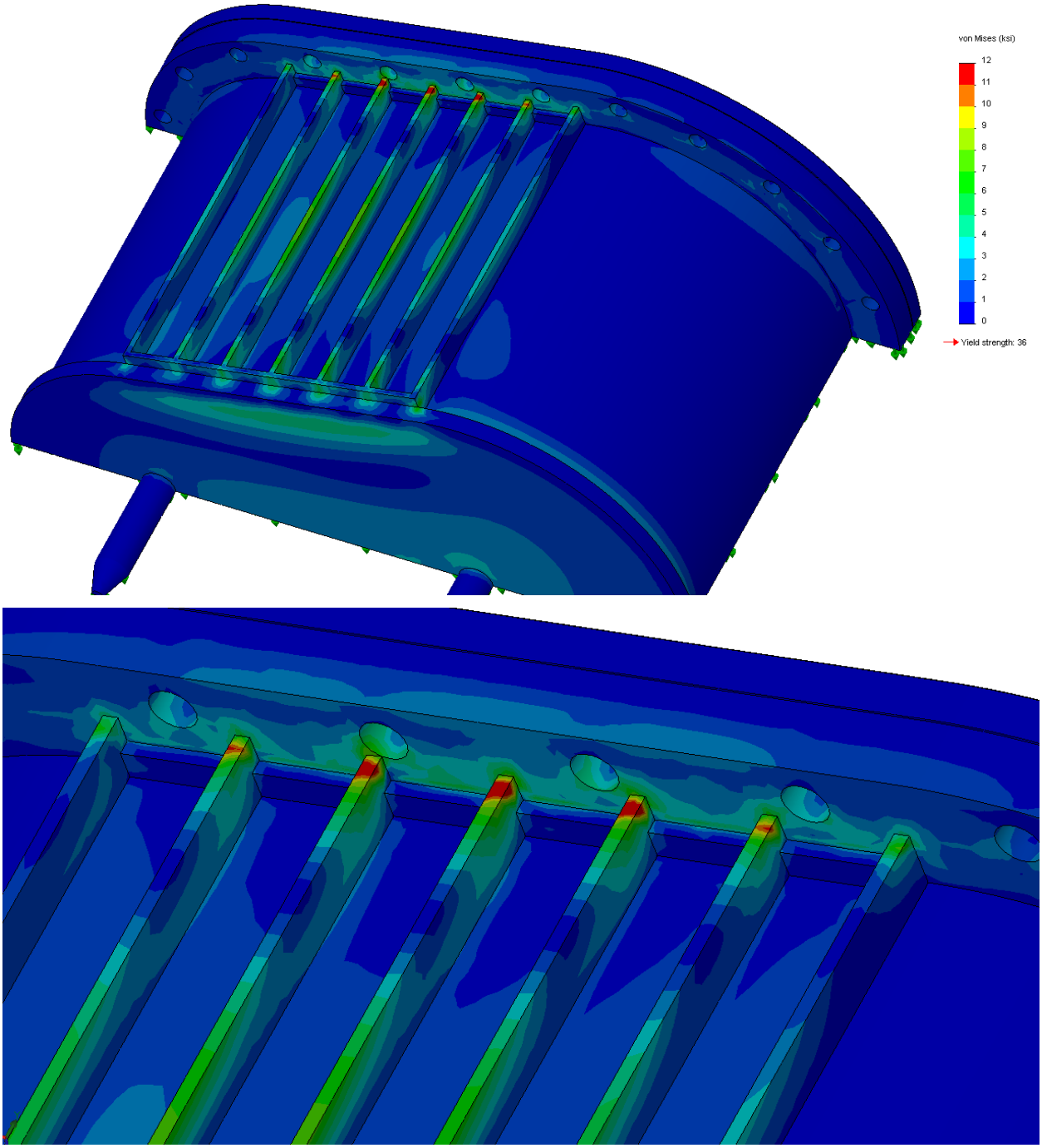

Fig. B.4. Stress results for the sump tank at 700°C, 30 psig. The lower image features the area where the struts join the tank, the highest stress region.

Creep and Rupture

The possibility of rupture has been removed based on the results shown in Fig. B.5. The view is taken perpendicular to the large face of the reinforcement struts. As none of the areas passes through the tank wall, rupture is not the likely failure mode.

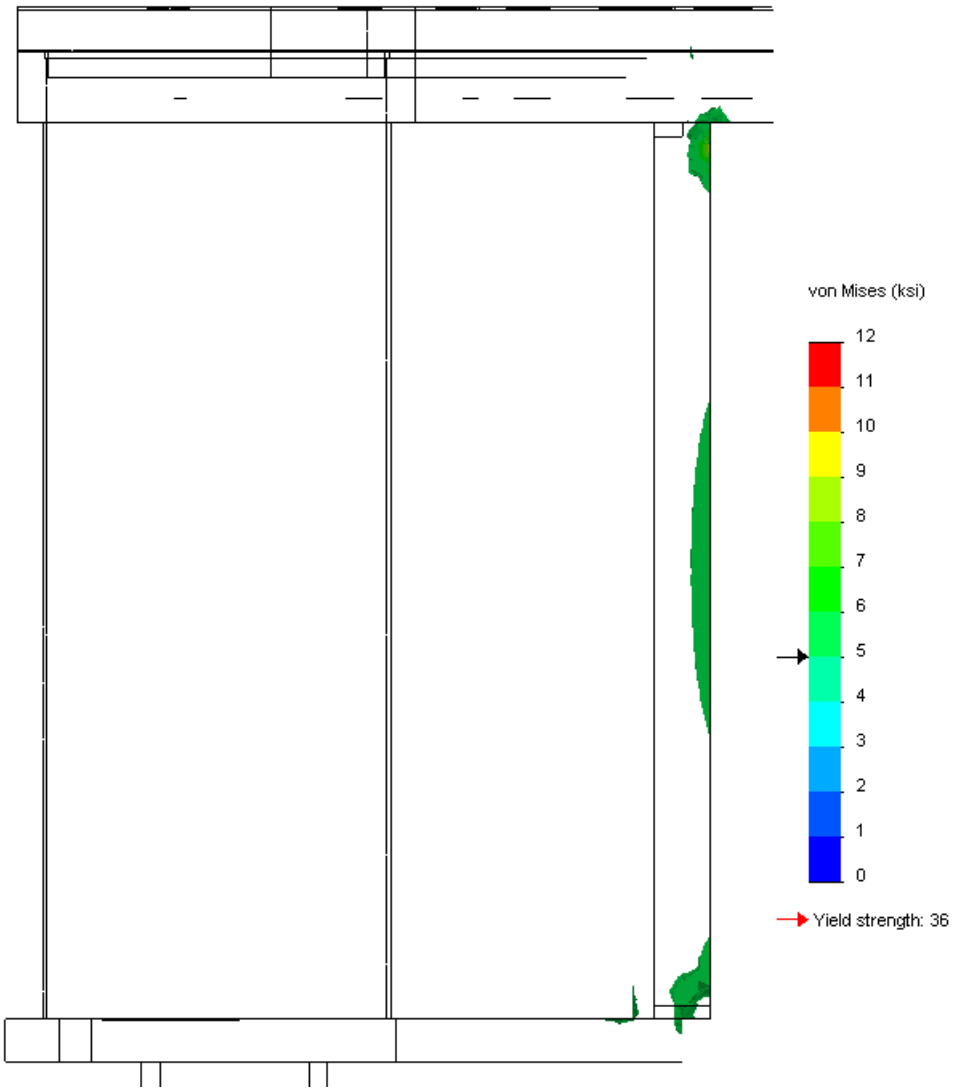

Fig. B.5. Areas above 5 ksi for 30 psig internal pressure. This will not rupture because the stress areas do not extend through the tank wall and primarily exist in the reinforcement bar.

Creep leading to a fracture must be assessed. Figure B.6 is a plot of the areas that exceed a 7 ksi stress, meaning that those areas are the only ones that will experience creep rates in excess of 0.06%/1000 h. All blue areas creep at or below this rate.

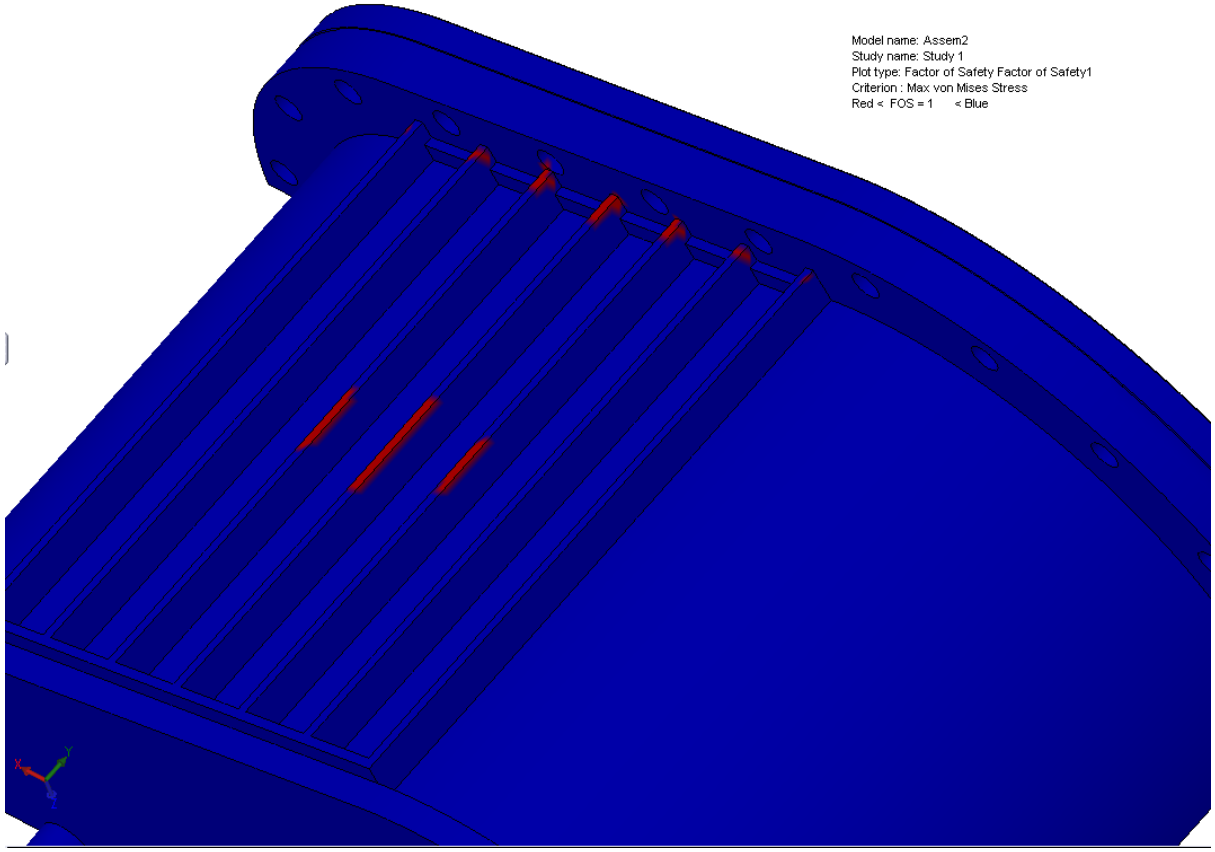

Fig. B.6. Areas above 7 ksi stress that are subject to creep rates that exceed 0.06%/1000 h (red).

45 psi Results

Compares the results at 30 psig and 45 psig (Figs. B.7 and B.8). All of the discussion above applies, but the risk of a failure increases. The same scale is used on both images.

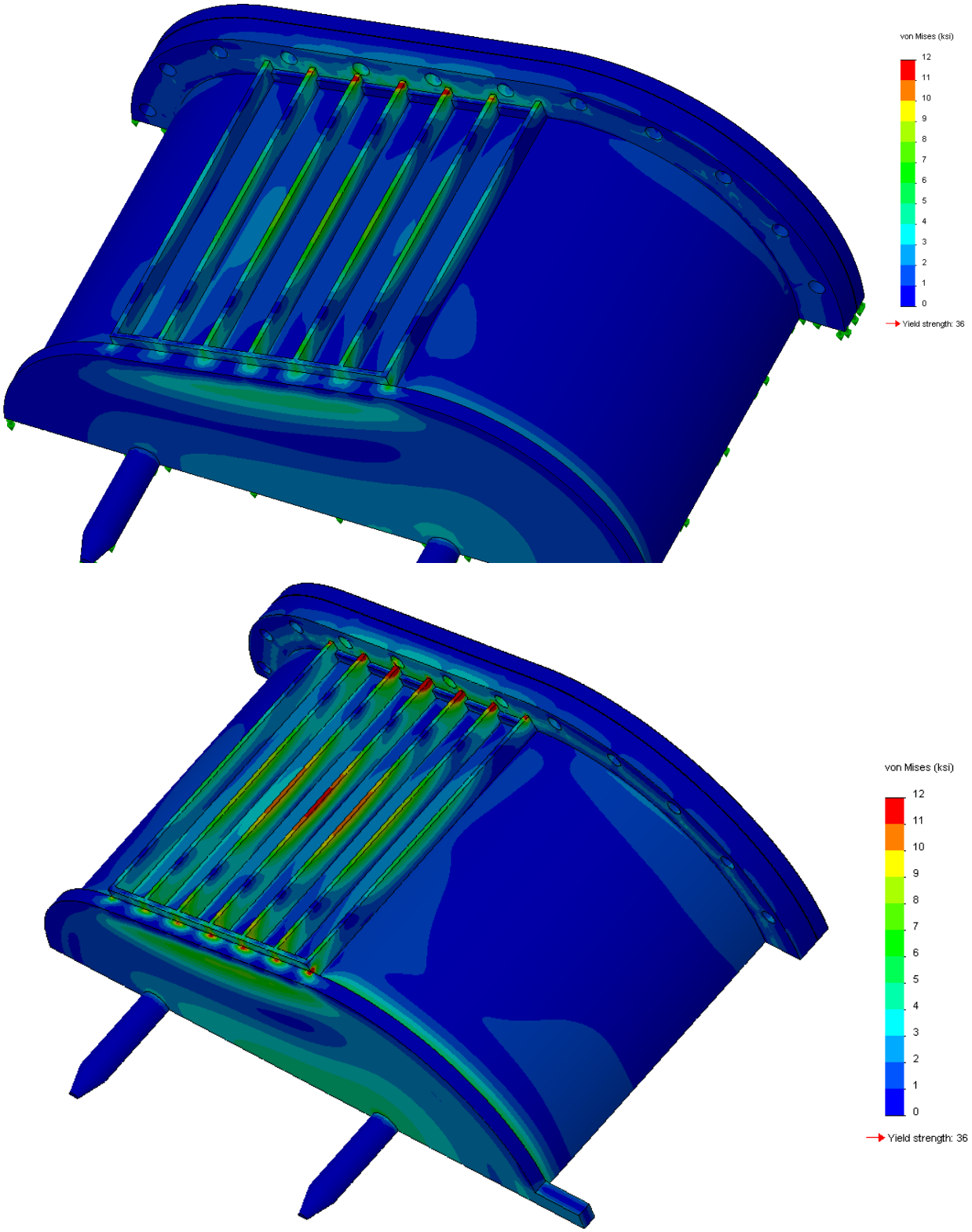

Fig. B.7. Stress plots for 30 psig (top) and 45 psig (bottom).

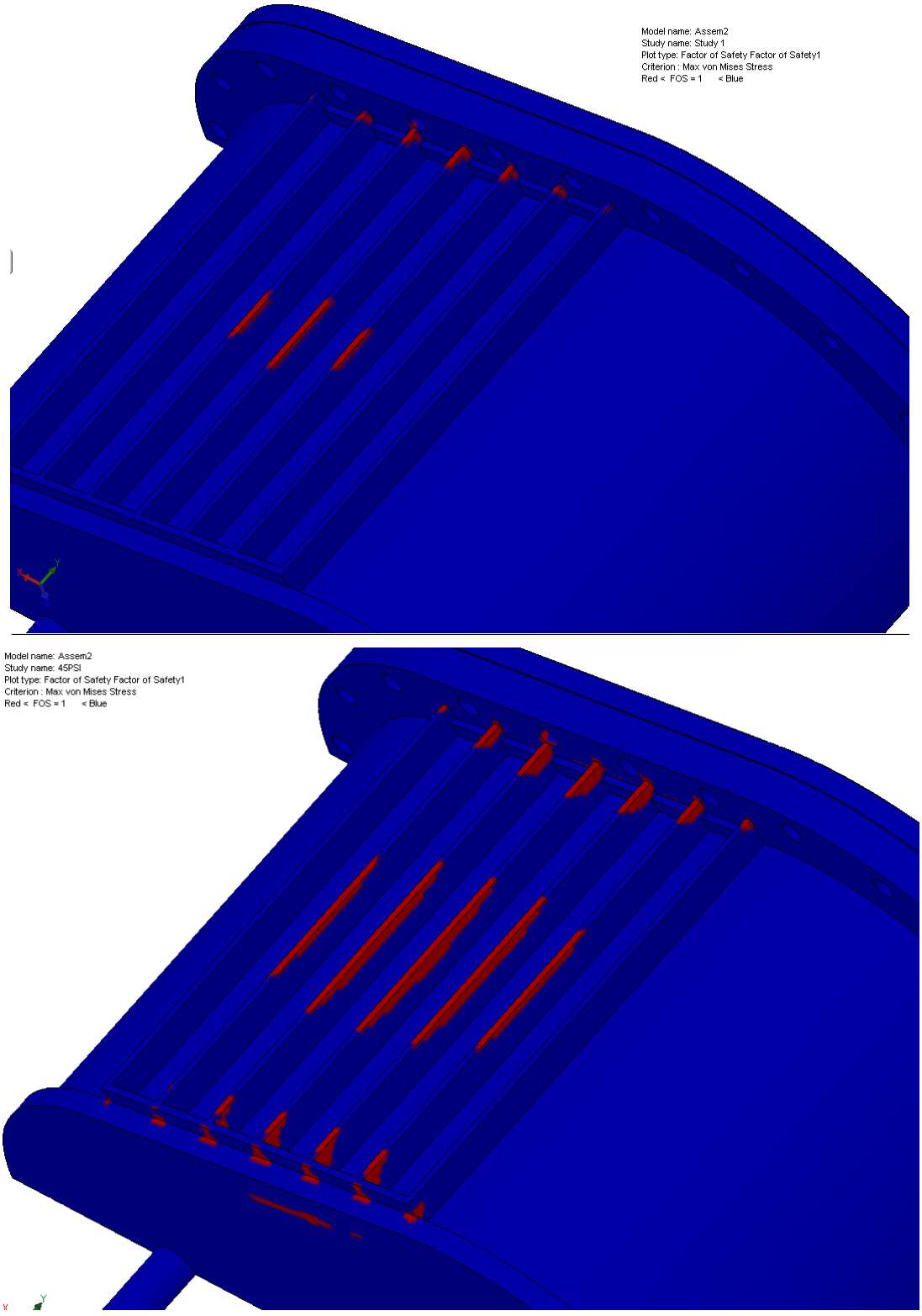

Fig. B.8. Areas in red exceed 7 ksi stress and are subject to creep rates in excess of 0.06%/1000 h.

APPENDIX C. PIPING STRESS CALCULATIONS

APPENDIX C. PIPING STRESS CALCULATIONS

Pressure calculations were performed for the storage tank, sump tank, and piping system. The surge tank will operate at pressures below 15 psig, and specific calculations for this tank were not performed.

Overview

The Molten Salt Test Loop at Oak Ridge National Laboratory consists of Inconel 600 piping and components. Inconel 600 was chosen for its compatibility with the FLiNaK salt that will be run through the test loop. Main loop components include a storage tank, sump tank, surge tank, test section, heat exchanger, rotary pump, piping, and pipe flange. Pipe stress analysis consisting of load stresses and displacements of the Inconel 600 piping and heat exchanger will be presented in this appendix.

Operation of the molten salt loop involves heating all wetted components to the FLiNaK melting temperature of 454°C. The loop is then filled and salt circulated to achieve the operating temperature of 700°C. Heating the loop from room temperature to 700°C causes considerable thermal expansion and structural stresses. The blue arrows shown below in Fig. C.1 denote the piping and heat exchanger that are discussed in this appendix.

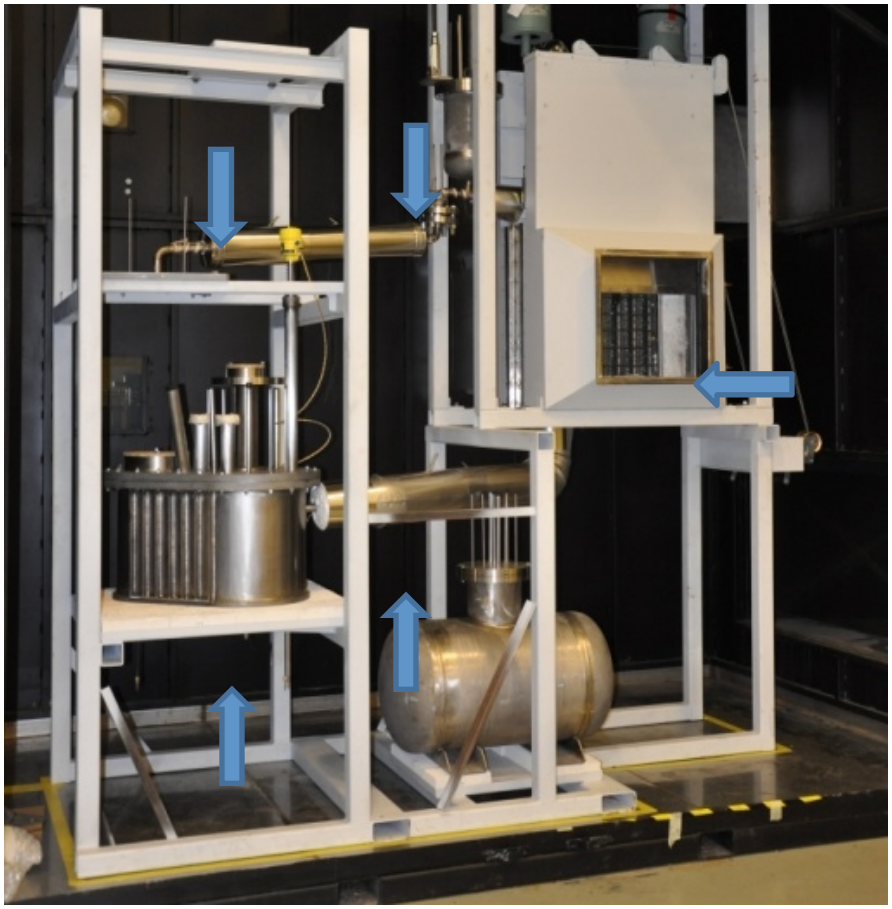

Fig. C.1. Molten Salt Test Loop.

Setup

CAEPipe software was used to model the salt loop section shown in Fig. C.1. Properties for Inconel 600 at room temperature and operating temperature were input into CAEPipe. Density, joint factors, Young's modulus, allowable pressure, and yield pressures were taken from www.specialmetals.com. These properties can be found in Table C.1. Allowable stresses were calculated according to American Society of Mechanical Engineers III Class 2 codes that set allowable stress at two-thirds of yield stress. CAEPipe software does not have the capability to model rectangular ducts and noncylindrical tanks. This was a problem when drawing up the heat exchanger tanks and sump tank that need to be analyzed in the salt loop. To create the model as accurately as possible, cylindrical tanks with the same volume and wall thickness as the heat exchanger tanks were modeled. To simulate expansion of the sump tank, 2 in. diameter solid Inconel 600 rods were put in place to limit deformation and provide an expansion force to the loop piping. Ideally the sump tank would be modeled to its true dimensions. Two rods were added to the model to represent the two support points on the sump tank. A 250 lb force was added to each support point to simulate the weight of the full sump tank during operation.

Table C.1. Inconel 600 properties from www.specialmetals.com

Temperature (°C)	25	700
Description	Inconel 600	Inconel 600
Type	Nickel alloys (NA)	Nickel alloys (NA)
Density (lb/in.^{3})	0.304	0.304
Nu	0.3	0.3
Joint factor	1	1
Young's modulus (psi)	3.11E+07	2.48E+07
Alpha (in./in./F)	5.80E-06	8.73E-06
Allowable (psi)	30,000	14,633
Yield (psi)	45,000	21,370

The salt loop being studied has six total supports: three hangers, two anchors, and one sliding pin. One hanger is located at the surge tank, and two more are located on the heat exchanger. All three hangers are identical Anvil International Spring Hangers Type C-268 size 10. Each hanger weighs 72 lb and provides a spring rate of 260 lb/in. Although the hangers appear upside down in Fig. C.2, they are providing a lifting force as intended. The first anchor is located at the top of the test section, where the loop piping is connected to the support framework of the salt loop. The second anchor is located at the bottom left side of the sump tank, where it is also pinned to the loop framework. A sliding pin is located at the bottom right side of the sump tank to allow the tank to slide in the horizontal direction when under thermal expansion. An internal fluid pressure of 15 psig was assumed in the main loop piping, and a lower pressure of 3 psig was assumed in the heat exchanger.

Four different pipe sizes were used in this model, shown below in Table C.2. Pipe 1 was used as the main loop piping, Pipe 2 was used as the heat exchanger tanks, Pipe 3 was used as the heat exchanger piping, and Pipe 4 was used as the sump tank.

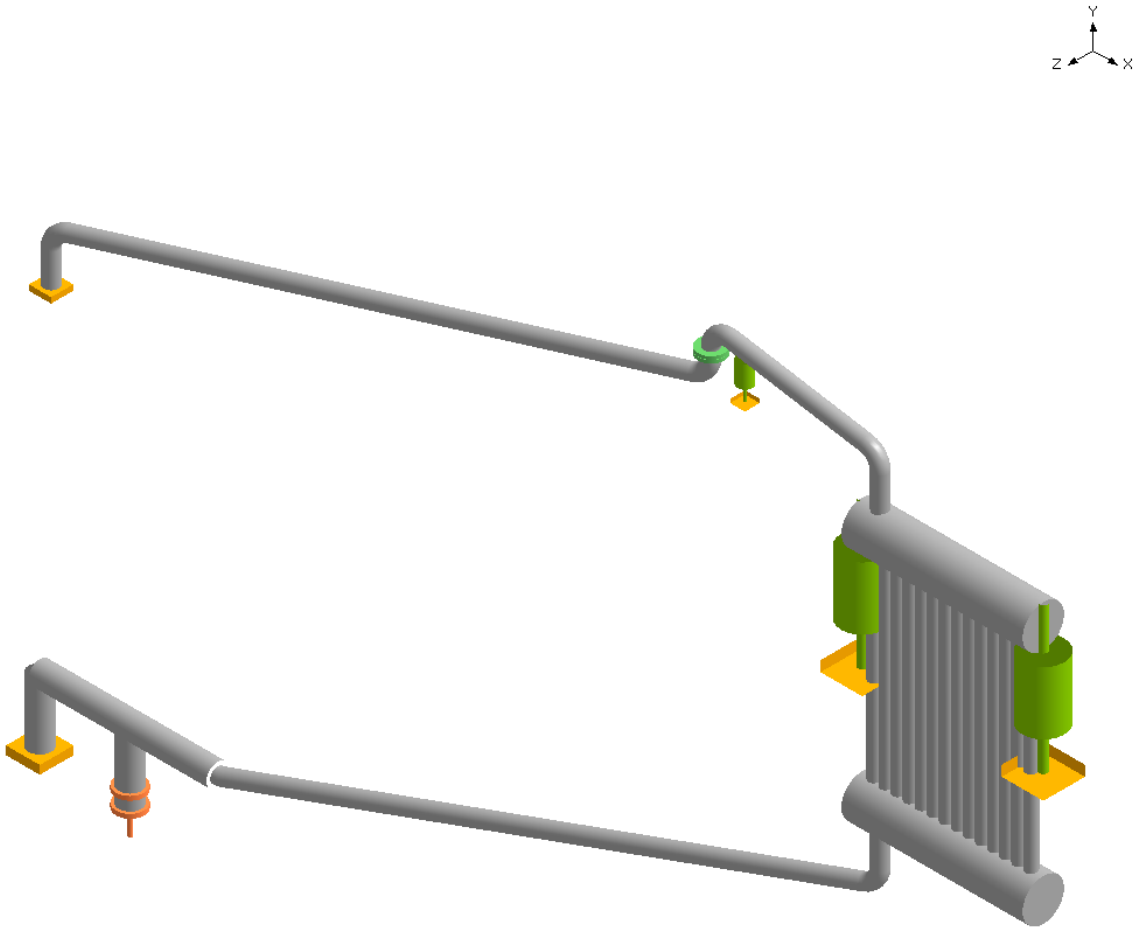

Fig. C.2. CAEPipe rendering of salt loop model.

Table C.2. Pipe sections used in salt loop model

Pipe name	Nominal diameter	Schedule	Outside diameter (in.)	Thickness (in.)
1	1 in.	40	1.315	0.133
2	Nonstandard		3.698	0.065
3	Nonstandard		1	0.065
4	Nonstandard		2	1

CAEPipe uses a Von Mises stress calculation that is based on distortion energy theory. Von Mises is a formula for calculating whether the stress combination at a given point will cause failure. When an element, such as a pipe, is subject to principle stresses σ_1, σ_2, the Von Mises stress is calculated $\sqrt{{\sigma_1}^2 - (\sigma_1 * \sigma_2) + {\sigma_2}^2}$ and compared to the allowable stress. Essentially, Von Mises stress is an equivalent stress calculated to determine if a combination of the principal stresses can cause failure.

Results

Stress diagrams shown below in Figs. C.3 and C.4 indicate the highest stress of 4514 psi at the first bend after Anchor #1. This stress is attributed to the entire loop expanding and moving up and to the right in the diagram, as shown in Fig. C.5. This places a maximum tension load of 4466 psi on the inner bend and a maximum compression load 4550 psi on the outer bend of the pipe. This point of stress does not pose a threat to the integrity of the loop piping as it is well under the allowable stress of 14,633 psi. Other notable stress points are the bends above and below the heat exchanger and the interface of the sump tank wall and loop piping. The bend directly above the heat exchanger experiences a maximum stress of 3242 psi. The bend directly below the heat exchanger experiences a maximum stress of 3154 psi. The sump tank-loop piping interface experiences a maximum stress of 2656 psi. All other stresses on the salt loop are negligible.

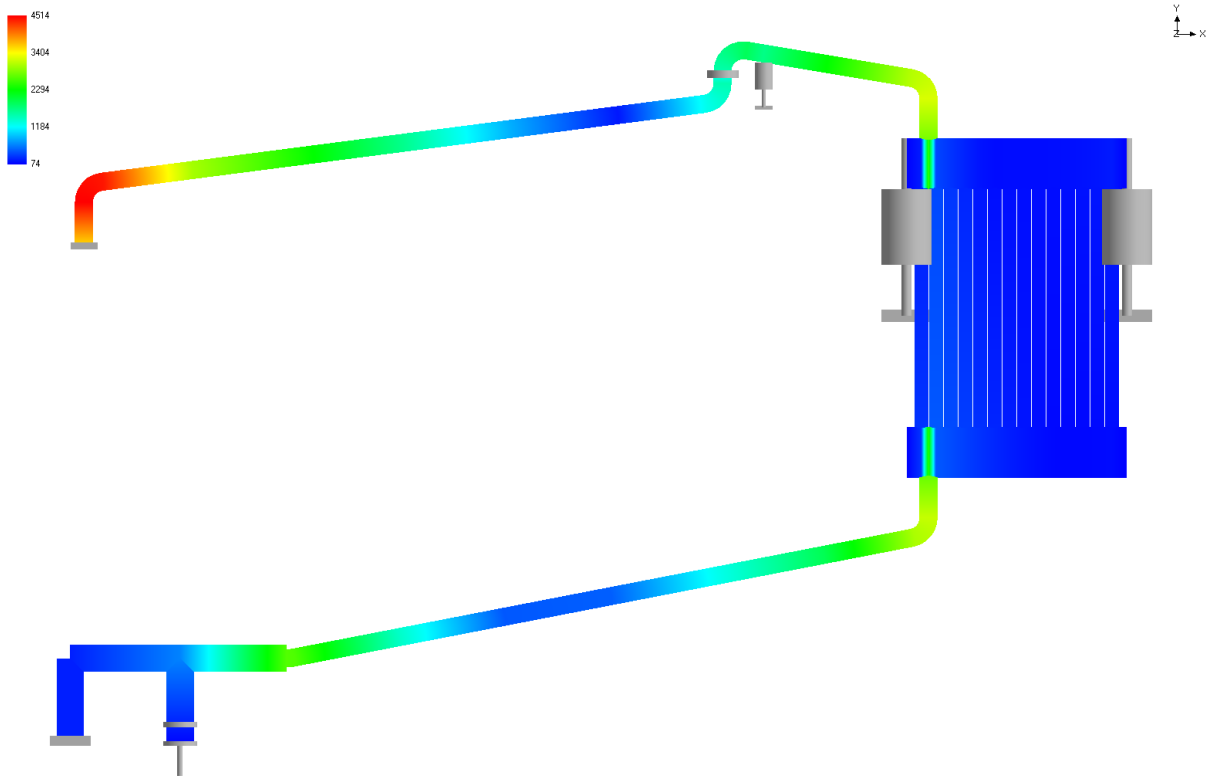

Fig. C.3. Von Mises stress (psi).

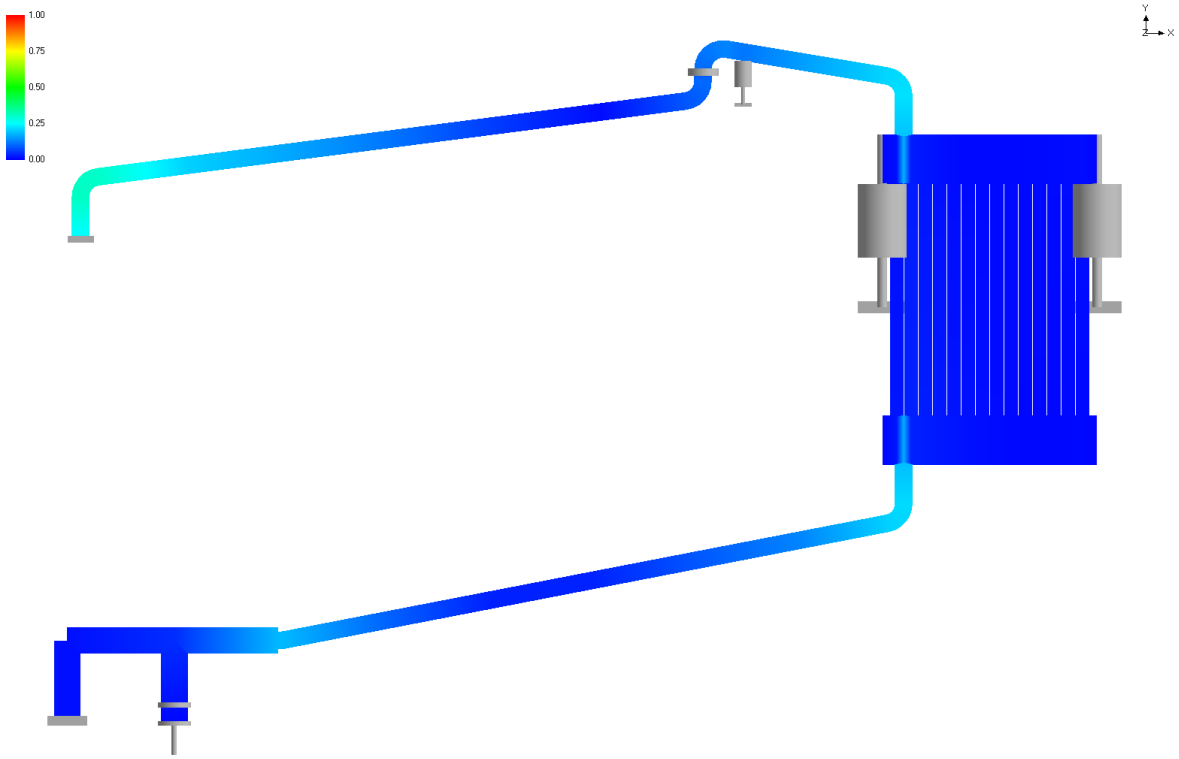

Fig. C.4. Von Mises stress to allowable stress ratio.

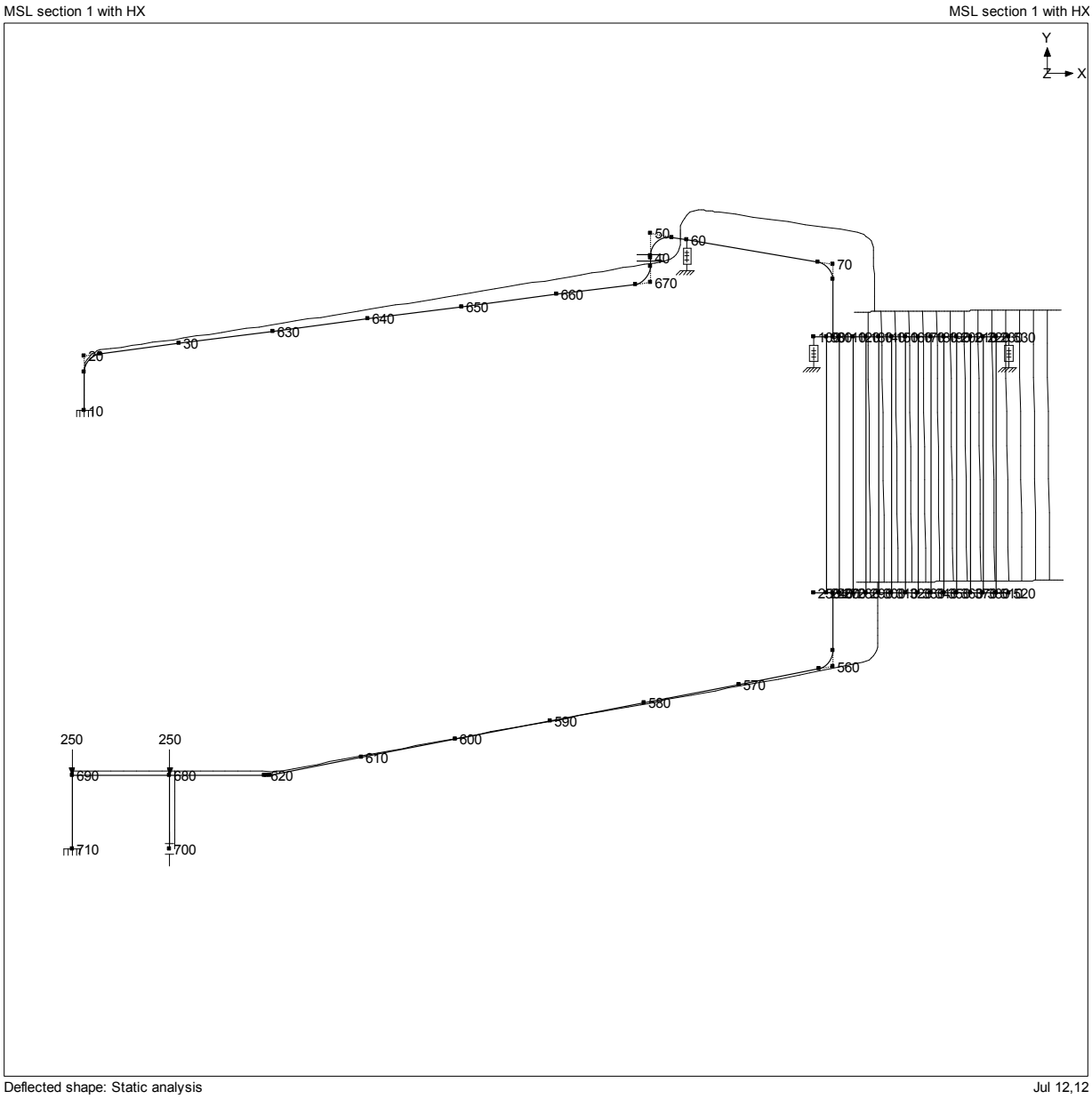

Fig. C.5. Nodal displacement of salt loop piping.

The stress ratio diagram shown in Fig. C.4 indicates a maximum stress ratio of 31% of allowable stress at the bend above Anchor #1. All other stresses are under 25% of the allowable stress.

A displacement diagram at operating temperature is shown in Fig. C.5. As the loop piping expands, it also moves in the vertical direction due to the force supplied by the hangers. Table C.3 lists the x,y, and z displacement for each node. Although Fig. C.5 appears to show significant displacement, no node moves more than 0.75 in. in any direction. Most displacement occurs in the X–Y plane, as shown in Fig. C.5.

Conclusion

After reviewing the aforementioned diagrams and CAEPipe output files, it is apparent that no additional supports are necessary on the salt loop piping. All stresses fall well within allowable limits and do not

require further action. Future work could consist of altering the model to calculate the number of cycles to failure and varying internal fluid pressure. Pressure drop across the heat exchanger and entire salt loop are in the process of being calculated using AFT Fathom.

Table C.3. Nodal displacement of molten salt loop

CAEpipe		MSL section 1 with HX		Page 1		
Version 6.4		MSL section 1 with HX		Jul 12,12		
Node	**X (in.)**	**Y (in.)**	**Z (in.)**	**XX(deg.)**	**YY(deg.)**	**ZZ(deg.)**
Displacements: Static analysis						
10	0.000	0.000	0.000	0.0000	0.0000	0.0000
20A	-0.001	0.033	0.000	0.0082	0.0017	0.0384
20B	0.010	0.050	-0.003	0.0247	0.0040	0.1133
30	0.075	0.077	-0.020	0.0397	0.0062	0.1881
630	0.151	0.120	-0.041	0.0540	0.0083	0.2630
640	0.225	0.172	-0.062	0.0637	0.0096	0.3194
650	0.299	0.230	-0.083	0.0679	0.0101	0.3544
660	0.372	0.292	-0.103	0.0660	0.0100	0.3653
670A	0.433	0.343	-0.121	0.0591	0.0093	0.3537
670B	0.438	0.367	-0.123	0.0514	0.0093	0.3309
Displacements: Static analysis						
40	0.434	0.374	-0.122	0.0504	0.0091	0.3283
50A	0.432	0.376	-0.122	0.0501	0.0091	0.3274
50B	0.442	0.401	-0.121	0.0429	0.0099	0.2954
60	0.456	0.405	-0.122	0.0407	0.0098	0.2886
70A	0.575	0.434	-0.124	0.0211	0.0081	0.2120
70B	0.593	0.423	-0.125	0.0143	0.0053	0.1594
80	0.604	0.374	-0.126	0.0075	0.0036	0.1180
90	0.599	0.373	-0.126	0.0075	0.0036	0.1179
100	0.588	0.371	-0.126	0.0075	0.0036	0.1179
110	0.610	0.375	-0.126	0.0074	0.0036	0.1177
120	0.621	0.377	-0.126	0.0073	0.0035	0.1173
130	0.632	0.379	-0.126	0.0071	0.0035	0.1170
140	0.643	0.382	-0.126	0.0070	0.0035	0.1167
150	0.654	0.384	-0.126	0.0069	0.0035	0.1166
160	0.665	0.386	-0.126	0.0068	0.0035	0.1166
170	0.676	0.388	-0.126	0.0067	0.0035	0.1166
180	0.687	0.390	-0.126	0.0067	0.0035	0.1166
190	0.698	0.392	-0.126	0.0066	0.0034	0.1167
200	0.709	0.395	-0.127	0.0066	0.0034	0.1168
210	0.720	0.397	-0.127	0.0065	0.0034	0.1170
220	0.731	0.399	-0.127	0.0065	0.0034	0.1171
230	0.742	0.401	-0.127	0.0065	0.0034	0.1171
240	0.641	0.156	-0.127	-0.0035	0.0016	0.1135
250	0.630	0.154	-0.127	-0.0035	0.0016	0.1135
260	0.647	0.157	-0.127	-0.0035	0.0016	0.1135
270	0.652	0.158	-0.127	-0.0034	0.0016	0.1138
280	0.663	0.161	-0.127	-0.0033	0.0017	0.1144
290	0.674	0.163	-0.127	-0.0032	0.0017	0.1148
300	0.685	0.165	-0.127	-0.0031	0.0017	0.1153
310	0.696	0.167	-0.127	-0.0030	0.0017	0.1156

Table C.3. Nodal displacement of molten salt loop (continued)

CAEpipe		MSL section 1 with HX		Page 1		
Version 6.4		MSL section 1 with HX		Jul 12,12		
Node	**X (in.)**	**Y (in.)**	**Z (in.)**	**XX(deg.)**	**YY(deg.)**	**ZZ(deg.)**
320	0.707	0.169	-0.127	-0.0029	0.0017	0.1158
330	0.719	0.171	-0.127	-0.0028	0.0017	0.1161
340	0.730	0.174	-0.127	-0.0028	0.0018	0.1162
350	0.741	0.176	-0.127	-0.0027	0.0018	0.1163
360	0.752	0.178	-0.127	-0.0027	0.0018	0.1164
370	0.763	0.180	-0.127	-0.0027	0.0018	0.1165
380	0.774	0.182	-0.127	-0.0027	0.0018	0.1165
510	0.785	0.184	-0.127	-0.0026	0.0018	0.1165
520	0.796	0.187	-0.127	-0.0026	0.0018	0.1165
530	0.753	0.403	-0.127	0.0065	0.0034	0.1172
560A	0.654	0.108	-0.126	-0.0116	-0.0001	0.0730
560B	0.644	0.092	-0.123	-0.0221	-0.0018	0.0227
570	0.576	0.080	-0.105	-0.0315	-0.0032	-0.0286
580	0.494	0.073	-0.084	-0.0385	-0.0043	-0.0731
590	0.412	0.071	-0.063	-0.0406	-0.0046	-0.0977
600	0.329	0.071	-0.042	-0.0368	-0.0042	-0.0994
610	0.246	0.068	-0.021	-0.0266	-0.0030	-0.0753
620A	0.167	0.061	-0.000	-0.0097	-0.0012	-0.0245
620B	0.163	0.061	0.000	-0.0074	-0.0009	-0.0131
680	0.083	0.062	0.000	-0.0046	-0.0007	-0.0039
690	0.000	0.062	0.000	-0.0017	-0.0004	0.0011
700	0.082	0.000	0.000	-0.0046	-0.0007	-0.0039
710	0.000	0.000	0.000	0.0000	0.0000	0.0000

APPENDIX D. LOOP PRESSURE DROP AND TEMPERATURE CALCULATIONS

APPENDIX D. LOOP PRESSURE DROP AND TEMPERATURE CALCULATIONS

Tubing and piping pressure drop

Pressure drop within the piping system was calculated using a friction factor for both turbulent and laminar flow, and the larger of the two friction factors was used.[1]

For turbulent flow ($Re_D > 2300$) the Fanning friction factor was calculated assuming flow through smooth pipe:

$$f = 0.0791/Re_T^{0.25}$$

for laminar flow ($Re_D<2300$)

$$f = 16/Re_T,$$

where the tube or pipe Reynolds number is defined as

$$Re_T = \rho V_T D_T/\mu$$

and

V_T = tube or pipe salt velocity and
DT = tube or pipe inner diameter.

Tubing and piping pressure drop, ΔP_T, was calculated as

$$\Delta P_T = 4 f \rho V_T^2/2*L/D_T,$$

where

L = piping length.

Similar calculations were performed for tubing runs in the heat exchanger.

Elbows in the piping were assumed to have a R/D_t of two, and the loss coefficient to friction factor ratio was given by[2]

$$K/f^* = -0.0002 (R/D_T)^5 + 0.0137 R/D_T^4 - 0.3215 (R/D_T)^3 + 3.4442 (R/D_T)^2 - 13.814 (R/D_T)+ 29.93,$$

where

R = elbow radius,
K = elbow loss coefficient, and
f* = Darcy friction factor.

The elbow pressure loss ΔP_E is calculated as

$$\Delta P_E = 4 (K/f^*) f \rho V_T^2/2.$$

Sudden expansions and contractions in the piping were assumed to lose one velocity head, ΔP_{Ex}, and one-half velocity head, ΔP_C, respectively.

$$\Delta P_{Ex} = \rho V_T^2/2$$
$$\Delta P_C = \rho V_T^2/2$$

Pebble bed pressure drop

Pressure drop through the pebble bed, ΔP_b, is calculated using the Ergun equation:[3]

$$\Delta P_b = \rho v_s^2 * (150*(1-\varepsilon)^2/Re_P/\varepsilon^3 + 1.75*(1-\varepsilon)/\varepsilon^3)*L_b/D_P,$$

where

ε = bed λιθυιδ fraction (taken as 0.4 in these calculations) and
L_b = bed length.

Pebble heat transfer

Heat transfer from the pebbles was calculated using a Nusselt number formulation by van Saden:[4]

$$Nu_p = 1.27\, k^{0.33}\, Re_P^{0.36}/\varepsilon^{1.18} + 0.033\, k^{0.5}\, Re_P^{0.86}/\varepsilon^{1.07},$$

where

k = salt conductivity.

The pebble heat transfer coefficient, *h* is then calculated:

$$h = Nu_p\, k/D_P.$$

With a pebble power of 1285 W and the loop operating at a flow rate of 4.5 kg/s, the temperature rise from salt to the surface of the pebble is approximately 53°C.

References

1. W.M. Rohsenow and H. Choi, *Heat, Mass, and Momentum Transfer,* Prentice-Hall, United Kingdom, 1961.
2. *AFT Fathom Users Guide*, AFI Fathom 8, 2011.
3. S. Ergun, "Fluid Flow through Packed Columns," *Chemical Process Engineering* **48**, 89–94 (1952).
4. van Staden, "Analysis of Effectiveness of Cavity Cooling System," 2nd International Topical Meeting on High Temperature Reactor Technology, Bejing, China, Sept. 22–24, 2004.